USGS Award Numbers 08HQGR0092-93

Collaborative research with URS, Corporation, California Geological Survey: Application of New Liquefaction Hazard Mapping Techniques to the Sacramento-San Joaquin Delta Area

FINAL TECHNICAL REPORT

SUBMITTED: APRIL 27, 2010 (REVISED)

December 23, 2009 (ORIGINAL)

Charles R. Real

California Geological Survey

801 K Street MS 12-31

Sacramento, CA 95814-3531

creal@conservation.ca.gov

http://www.conservation.ca.gov/cgs

Keith L. Knudsen

URS, Corporation

1333 Broadway, suite 800

Oakland, CA 94612

keith_knudsen@urscorp.com

NEHRP Element: I and III

Key Words: liquefaction hazard maps, deformation approach, displacement potential index, Sacramento-San Joaquin Delta

Research supported by the U.S. Geological Survey (USGS), Department of the Interior under USGS award number (08HQGR0092 and 08HQGR0093). The views and conclusions contained in this document are those of the authors and should not be interpreted as necessarily representing the official policies, either expressed or implied, of the U.S. Government.

Abstract

Liquefaction hazard maps have been prepared for the native levee foundation sediments (levees not evaluated) in the central Sacramento-San Joaquin Delta region. The hazard assessment is based on deformation potential of the sediments expressed as the capacity for horizontal displacement from limiting shear-strains caused by earthquake-induced cyclic shear stresses during shaking. The approach has the distinct advantage of portraying hazard in terms that relate to the potential for structural damage and attendant losses rather than only the potential for the occurrence of liquefaction.

Research in this project advanced the development of strain-based methods of mapping liquefaction hazard beyond results from previous work by the authors, funded by the Pacific Earthquake Engineering Research Center, allowing for more knowledge of the three-dimensional spatial distribution of liquefiable subsurface sediments to reduce epistemic uncertainty in the mapping of liquefaction hazard. Recently improved relationships between fines-corrected penetration resistance, induced cyclic stress ratio, and shear- and volumetric -reconsolidation strain forms the fundamental basis for the methodology. Unconsolidated Quaternary geologic map units are reclassified into liquefaction susceptibility units based on statistical similarity of strain-depth functions calculated from over 3,000 borehole penetration tests. Strain-depth density functions are then computed by grouping all borehole information within a defined liquefaction susceptibility unit, and parametrically modeling liquefaction response by varying shaking input assuming 100% saturation of sediments. The set of resulting strain-depth density curves are then integrated over the thickness of subsurface liquefiable sediment layers to estimate displacement potential. The final hazard maps represent hazard as lateral displacement and volumetric-reconsolidation potential expressed as interval ranges of displacement indices.

Non-Technical Summary

Settlement and horizontal shifting of the ground caused by liquefaction during earthquakes can result in serious damage to the foundation of buildings, bridges, pipelines, and other engineered structures. Advanced knowledge of where liquefaction is likely to occur can help prevent such losses by targeting areas to avoid or building stronger foundations and improving the ground. A new method of mapping where such damaging ground failures are more likely to occur during earthquakes has been developed that can improve land-use and construction decisions, resulting in safer development.

Table of Contents

1 Introduction 5
1.1 Background and Purpose 5
1.2 Previous Seismic Vulnerability Studies in the Delta 5
1.3 General Approach 7
1.4 Target Products 8
1.5 Previous work 8
1.6 Deformation Mapping 9
1.6.1 Outline of Procedure 9
1.6.2 Modifications to the “Proposed” Procedures 15
1.7 Principal Tasks 16
2 Analysis 16
2.1 Data Collected 16
2.2 Development of Database 17
2.3 Subsurface Stratigraphic Analysis 17
2.3.1 Definition of Working Stratigraphic Units 20
2.3.2 Preparation of Paleo-land Surface Map 21
2.4 Boring Log Deformation Analysis 23
2.4.1 Removal of Levee Overburden 23
2.4.2 Parametric Modeling of Borehole Response 23
2.5 Liquefaction Susceptibility 26
2.5.1 Existing Surface Geology 26
2.5.2 Paleo-Land Surface Geology 29
2.6 Ground Shaking 32
2.6.1 Peak Ground Acceleration 32
2.6.2 Liquefaction Opportunity 32
3 Results 32
3.1 Principal Subsurface Units 32
3.1.1 Non-liquefiable Units 34
3.1.2 Liquefiable Units 37
3.2 Liquefaction Deformation Potential 37
3.2.1 Liquefaction Deformation Potential Functions 37
3.2.2 Liquefaction Deformation Hazard Maps 44

4 Discussion 48
4.1 Significance of Results 48
4.2 Limitations 49
4.2.1 Data 50
4.2.2 Method 51
4.3 Recommendations for Further Work 53
5 References 54
6 Plates 56
6.1 Paleo-land surface on the base of the peat-soft organics 56
6.2 Large-scale geologic map of paleo-land surface 56
7 Acknowledgments 56

Delta Technical Report

1 Introduction

1.1 Background and Purpose

The Sacramento-San Joaquin Delta is an integral part of California's landscape that is exposed to significant earthquake hazards. Beside the critical ecosystem benefits it provides, about ¼ of urban water used in California comes from the Delta and a significant part of the state's agriculture depends on the Delta for its water. Although the current population is relatively small compared to other urban areas exposed to earthquake hazards in California, there are rapidly growing communities on the margins of the Delta. The Delta also is the home to many lifeline and utility corridors, which, if damaged, would severely impact California's economy and standard of living. There are more than 1,000 miles of levees in the Delta. These levees are different than most flood control levees in that they hold back the sea (much of the Delta lies below sea level) every day, rather than just functioning during flood events. In this project, we assess the liquefaction hazard to levee foundation materials (natural deposits) for a part of the Delta (Figure 1) and we evaluate the usefulness of a new approach as a means of identifying hazardous areas as the long-term future of the Delta is planned.

This project is a collaborative effort between the California Geological Survey (CGS) and URS Corporation (URS), and as such consists of two complimentary NEHRP-funded projects with work distributed in the following manner: (a) CGS developed a geotechnical database of boring logs throughout the Delta, analyzed the data for liquefaction potential using recent standardized procedures, and estimated deformation potential using a newly developed approach, and (b) URS interpreted geologic and geomorphic information to develop models that characterize the distribution of liquefiable materials, which is used to extrapolate and interpolate parameters used to assess liquefaction potential and forms the basis for mapping hazard over the study area. This report presents results of both parts of the joint study.

1.2 Previous Seismic Vulnerability Studies in the Delta

Recent work regarding earthquake vulnerability of the Delta includes studies sponsored by the California Department of Water Resources: CALFED Bay Delta Program (BDP) "Seismic Vulnerability of the Sacramento–San Joaquin Delta Levees" (CALFED, 2000), the CALFED Ecosystem Restoration Program (ERP) "Geomorphic and Geologic Mapping for Restoration Planning Sacramento-San Joaquin Delta Region" (Hitchcock et al., 2005), and the Delta Risk Management Strategy (DRMS) (URS, 2008). Although these studies focused on levee vulnerability, to our knowledge, a map of Delta liquefaction hazard has not previously been created and the DRMS reports have not produced hazard assessments that are spatial in

nature for levee foundation materials (e.g. hazard maps showing degrees of hazard and how the hazard varies throughout the Delta).

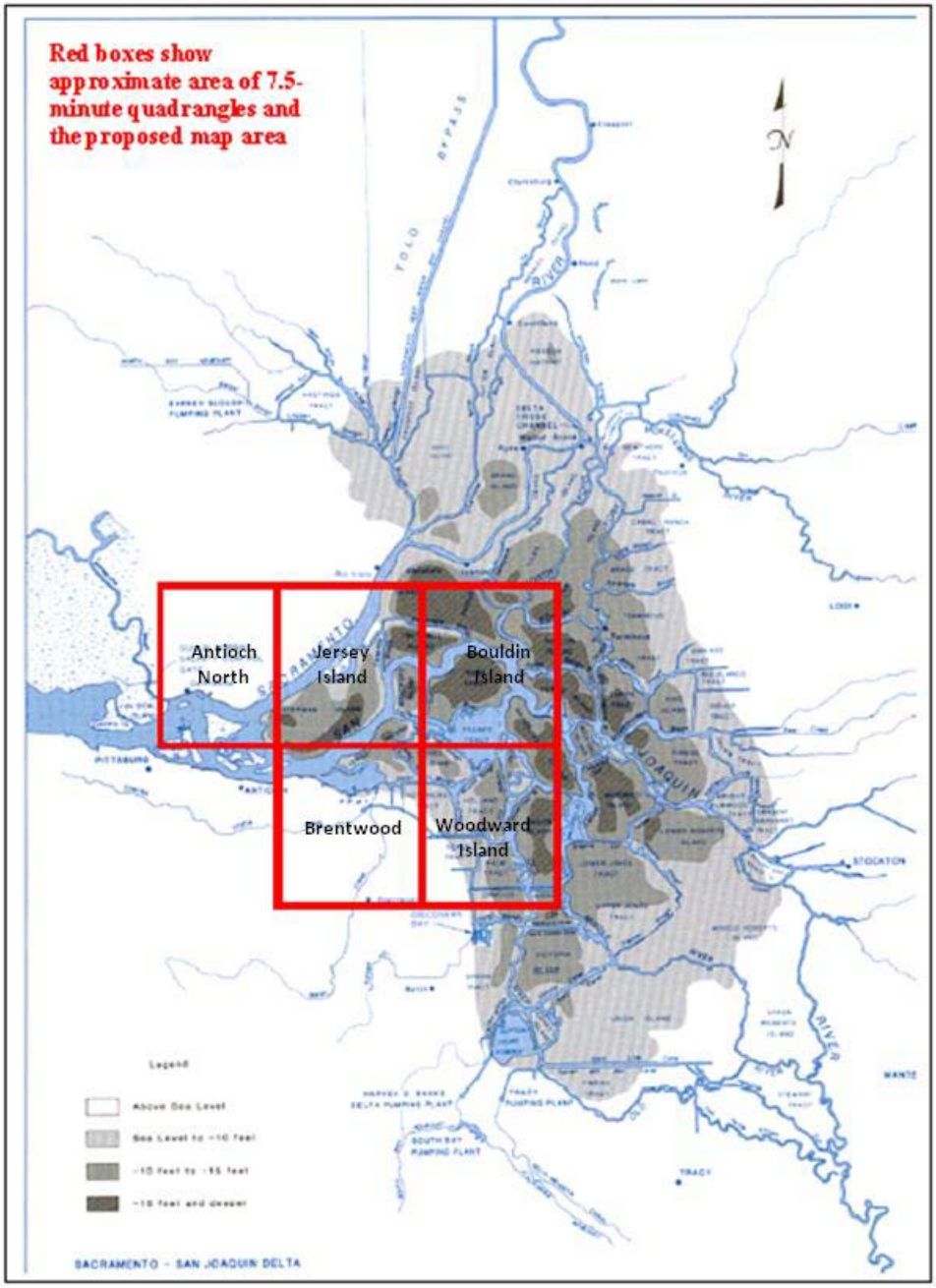

Figure 1. Land Surface below sea level in the Sacramento-San Joaquin Delta and project map area. Modified from Sacramento San Joaquin Delta Atlas, DWR, 1995.

The CALFED BDP study included a probabilistic seismic hazard analysis considering alternative source models in order to estimate 100-yr return period ground motions that were input to a

fragility analysis of 34 levee locations in the Delta. One source model was equivalent to the 1996 CGS Model (Peterson et al, 1996), which includes the Coast Range–Central Valley blind thrust, the other source model removed the latter, but includes the Midland fault source that runs through the Delta (WLA, 1998). Failure analysis included both liquefaction and non-liquefaction mechanisms, and results are portrayed as probability of exceedance of number of levee failures for exposure times of 50-yr, 100-yr, and 200-yr. Each analysis included levee foundation material; however, results indicate that levee fragility is predominantly dependant on material strength within the levees. The study also delineates four damage potential zones based on the presence of loose, cohesionless sandy and silty levee materials and soft foundation materials. The highest potential corresponds to Sherman Island, the second highest to the central Delta region, the third highest the southern Delta region, and the lowest the northern Delta region.

The CALFED ERP study was designed to compile an extensive digital GIS database of existing geologic mapping, with new mapping on the distribution of historical deposits from flood events and hydraulic mining activity based on analysis of vintage aerial photographs and topographic maps. The result is a comprehensive geological database for future Delta restoration work, which proved to be very valuable in this project.

The DRMS study is a currently on-going large-scale, broad-scope evaluation of “stress factors” causing change in the Delta environment or placing the future integrity of the Delta ecosystem and fresh-water conveyance at risk, addressing: seismic, flood hazard, wind wave, climate change and sea-level rise, among other factors. Work includes an up-dated, more comprehensive levee fragility analysis incorporating the latest developments in PSHA, detailed geotechnical sampling and analysis of levee stability using non-linear finite difference code. A database of nearly 2,000 boring logs was interpreted for analysis of foundation and levee performance for several different failure modes including liquefaction and non-liquefaction mechanisms.

1.3 General Approach

The approach taken in this study takes advantage of the data and analyses from the above previous work and begins with application of a methodology developed under a Pacific Earthquake Engineering Research Center (PEER) research grant. Lithology, soil indices and penetration data from boring logs are evaluated for liquefaction deformation potential expressed in terms of shear-strain and volumetric-reconsolidation potentials as a function of depth (liquefaction response functions). These data are then statistically evaluated for significant differences, and the results used to reclassify surface geological mapping in terms of liquefaction deformation potential. Hazard potential is defined on the basis of potential for shear deformation (lateral displacement) without regard to static driving stresses. Each unit’s liquefaction response to earthquake shaking can then be modeled parametrically to produce a “hazard potential function” (HPF) for which the independent variables can be mapped spatially from data contained in boring logs. The key is to use the HPF to integrate maps of the independent variables into an estimate of strain potential and subsequently displacement potential given total thickness of liquefiable materials, depth of saturation and estimated ground shaking.

Usually, a depth to saturation (first water encountered) is acquired from previous studies or produced from boring log data. Previous work indicates that groundwater in the study area lies at depths of 2 and 3 feet below the ground surface. In this project, we assume the water table is uniformly at the ground surface. To better understand the potential for liquefaction, subsurface stratigraphy is analyzed to estimate thicknesses of liquefiable material, and to map the base of the peat deposits. We investigate the feasibility of mapping the geomorphology and geology of the paleo-land surface on which peat was deposited beginning six to eight thousand years ago, in an attempt to better understand geomorphic controls on sand deposition. That information is used to help define and map units susceptible to liquefaction.

1.4 Target Products

Key products resulting from the study include 1) correlated multi-log sections that are interpreted in terms of liquefiable and non-liquefiable materials, 2) maps of the paleo-land surface prior to sea level rise and deposition of peat, 3) isopach maps of liquefiable and non-liquefiable material, 4) database of liquefaction deformation analysis results for borings having penetration tests, 5) maps showing levels of liquefaction susceptibility based on strain potential, and 6) hazard potential maps based on deformation potential.

1.5 Previous work

Early methods of mapping liquefaction hazard over large areas have mostly relied upon geological and geomorphological criteria that relate to the depositional environment and age of deposits and field performance during past earthquakes (Youd and Perkins, 1978). Once the potential for liquefaction failure of geologically youthful deposits has been categorized, their mapped distributions are then used to extrapolate hazard susceptibility over the area of interest. Recent efforts have improved that approach by facilitating the ranking of hazard susceptibility by using more field measurements such as standard penetration and cone penetrometer tests and liquefaction potential index (Witter et al., 2006; Holzer et al., 2006). Such assessments primarily reflect the potential for onset of liquefaction, with little beyond an ordinal ranking for liquefaction occurrence susceptibility and how severe the surface ground deformation might be.

Previous methods of estimating liquefaction deformation have followed three approaches: 1) empirically-derived relationships for predicting lateral spread displacement, 2) physics-based site-specific approaches using nonlinear, strain-history finite element and finite difference methods, and 3) hybrid methods. Previous research conducted by the authors funded by the PEER and CGS demonstrates that, with suitable detail in mapping of Quaternary sediment deposits and abundant geotechnical penetration test measurements, it is possible to characterize the spatial variability of sediment strain potential, and to regroup surface geologic map units (or subdivide them) into liquefaction susceptibility units that have statistically different liquefaction responses (Real et. al, 2008). The procedure consists of analyzing a soil column by identifying which sediment layers in a borehole liquefy under a given seismic demand using a standardized “simplified method” (Youd et al., 2000; Cetin et al., 2004) and estimating the amount of strain based on empirical relations derived from measurements in the field and laboratory. The strain is then multiplied by the liquefied layer thickness and summed layer by layer to yield the amount of liquefaction-induced displacement expected at the site. Recent work has extended this approach to estimating displacement potential due to both volumetric

and shear strain, and for large as well as small displacements calibrated against field observations (Faris, 2004; Seed et al., 2003; Wu, 2002). Unlike liquefaction potential index, the displacement potential index has provided a basis for mapping potential deformation in quantitative units that make physical sense (Knudsen et al., 2004a, 2004b; Rosinski et al., 2004).

Expanding on early work by Tokimatsu and Seed (1987), Ishihara and Yoshimine (1992), and Shamoto and others (1998), Wu (2002) developed new charts for estimating limiting shear strain as a function of $N_{1,60,cs}$ and induced cyclic stress-ratio based on extensive undrained, cyclic shear testing of fully saturated sand. Faris (2004) calibrated these charts against field observations, and introduced the displacement potential index (DPI) as a hazard deformation parameter, which simply sums the estimated shear displacements of each layer that liquefies in a soil column to yield a total displacement. A regression formula based on DPI and slope gradient as a proxy for static driving stress also was developed for estimating horizontal displacement (Faris et al., 2006). Zhang and others (2004) developed a similar approach and produced a lateral displacement index (LDI) based on simplified liquefaction analysis of SPT or CPT data, and integrating induced cyclic shear stress with depth.

We chose the method of Faris (2004) and calculate DPI in order to characterize liquefaction deformation potential for mapping liquefaction hazard in the Delta.

1.6 Deformation Mapping

In this study we expand on methods developed under PEER-supported research (Knudsen et al., 2004b), and map liquefaction deformation-susceptibility and potential using the concept of strain-depth curves (Real et al, 2008). Like previous approaches, we use geologic maps to extrapolate hazard throughout the geographic area, but calibrate it in a quantitative way that reflects the sediment body's capacity for permanent surface deformation as a function of 1) thickness of liquefiable material (considering penetration resistance, fines content, soil type, etc.), 2) depth to sediment saturation, and 3) level of shaking. A key feature of our approach is that by isolating these three independent variables and mapping them separately more of the spatial variability of liquefaction can be accounted for. Areal grids of these three parameters are prepared and integrated to yield shear-strain and displacement grids for the mapping area. The method requires abundant geotechnical boring logs that are well distributed spatially and detailed Quaternary geologic maps that delineate sediments with respect to the age and environment of sediment deposition. Quaternary geology map units are reclassified into susceptibility units based on their liquefaction response. Although primarily a two-dimensional approach, variability of surface unit response at depth is modeled parametrically, the results of which become a multi-dimensional lookup table to yield strain and displacement indices at a point on the ground surface.

1.6.1 Outline of Procedure

The liquefaction mapping method consists of five basic steps as illustrated in Figure 2: 1) Analysis of boring logs to yield depth of basement, depth to saturation, and required geotechnical parameters (soil indices, penetration resistance, unit weights, etc.), 2) Assessment of liquefaction opportunity (magnitude-weighted peak ground acceleration on alluvium), 3)

Analysis of boring log sediment susceptibility to liquefaction and geologic unit reclassification, 4) Analysis of liquefaction potential and development of a hazard potential matrix, and 5) Calculation of shear-strain and displacement potential grids that represent hazard over the map area.

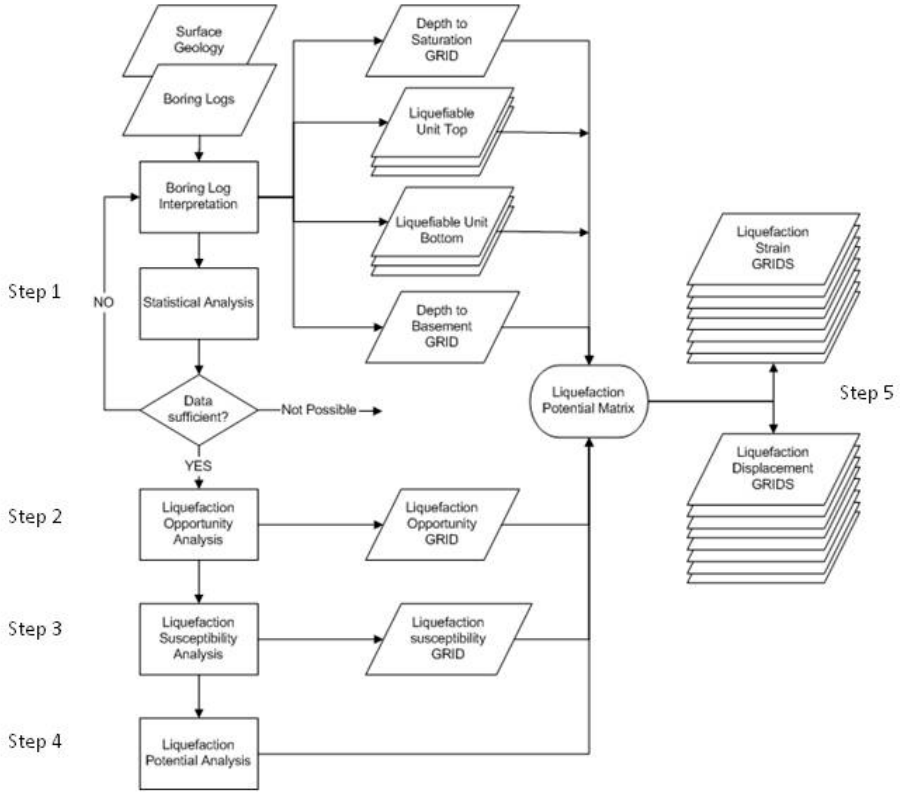

Figure 2. Liquefaction deformation mapping procedure. Note that the current research modified the original process by adding a component of subsurface stratigraphic analysis that defines position and potential deformation of potentially liquefiable strata (liquefaction unit top and bottom layers above; modified from Real and others, 2008).

Step 1 - The first step is to collect and interpret boring logs to estimate depth to sediment saturation and depth to "liquefaction basement." Liquefaction basement is defined as bedrock or a prescribed depth below which liquefaction is not expected to occur. The results are used to prepare depth-to-liquefaction basement and depth-to-saturation grids over the region by interpolating a continuous surface between boreholes. Geostatistical analysis of borehole spatial distribution can be used to determine adequacy and character of sampling so sufficient data and appropriate methods of interpolation can be identified. This type of analysis is common practice in the exploration of mineral and petroleum resources and for groundwater resource and environmental studies, and provides a mapping of subsurface parameters over a

study area. The first step also includes statistical analysis of measured geotechnical parameters and their derivatives, such as $N_{1,60,cs}$ and response parameters such as strain potential index (SPI) and displacement potential index (DPI) (Faris, 2006; Seed et al., 2003; Wu, 2002), which are used to calibrate and reclassify liquefaction response of surficial geology map units.

A principal component of the proposed mapping methodology involves parametric modeling of the liquefaction response of the soil column represented by each boring log in terms of SPI. SPI requires calculation of liquefaction potential according to the simplified method to yield induced cyclic stress ratio (CSR) and $N_{1,60,cs}$ for each liquefied layer identified in the boring log. These parameters are then used to estimate SPI from the limiting shear-strain potential curves shown in Figure 3 for each layer that liquefies.

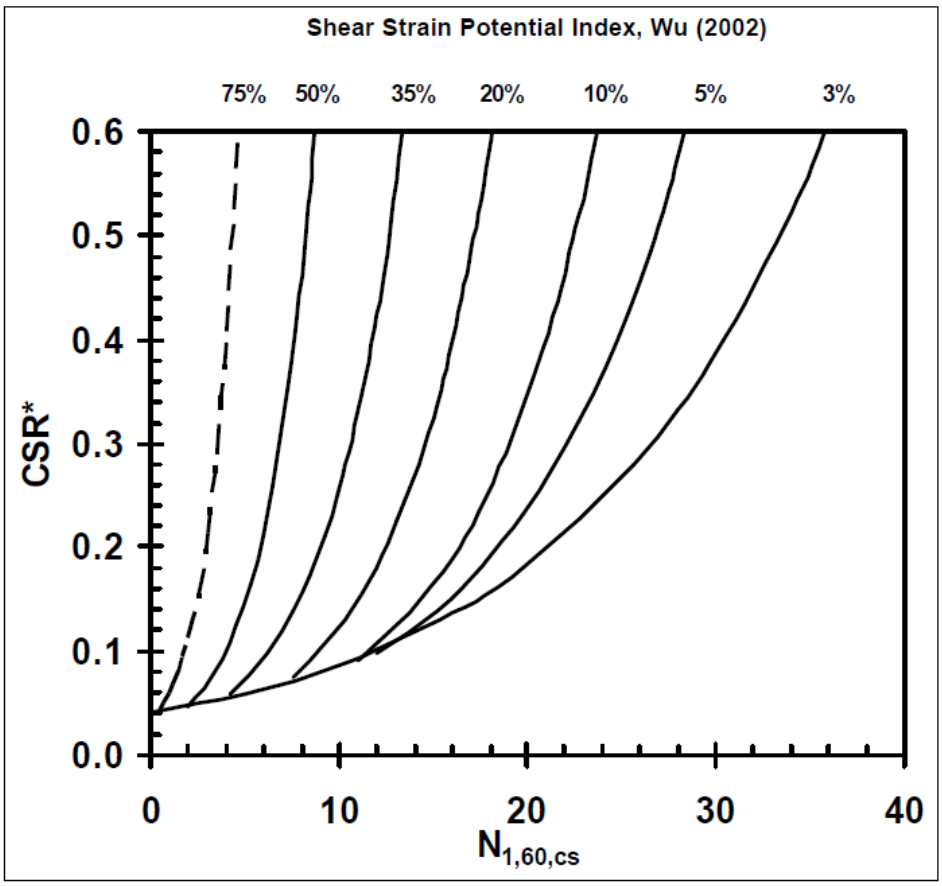

Figure 3. Shear-strain potential (modified by Faris, 2006).

Multiplying SPI by the layer thickness yields displacement potential of each liquefied layer. Summing displacement of each liquefied layer from the ground surface to a prescribed depth

and dividing by that depth yields shear-strain potential for that portion of the soil column according to the following equation:

(1) $\varepsilon(z) = 1/z \sum H_i * SSTRAIN(CSR, N_{1,60,cs})$ for i = 1, to number of liquefied layers to depth z

where, H is thickness of liquefied layer, CSR is induced cyclic stress ratio, $N_{1,60,cs}$ is normalized fines-corrected blowcount, and SSTRAIN is a functional form of Figure 3, shear-strain potential.

Modeling is accomplished by progressively incrementing the level of shaking and depth-to-saturation over a prescribed range in the calculation of liquefaction potential, and computing shear-strain potential repeatedly for prescribed depth ranges and for all combinations of independent variable values using equation 1. For clarity, we note that the term “depth range” means depth measured from the ground surface to a prescribed point below the ground surface. This yields a 3-D liquefaction boring response matrix of shear-strain potential for prescribed intervals of ground shaking, depth-to-saturation, and thickness of soil column for each boring log. These data are key derivative parameters for estimating liquefaction hazard susceptibility and hazard potential. Step 1 is completed when a sufficient number of boring logs having the necessary geotechnical parameters and suitable spatial sampling are acquired that will allow statistically significant correlation with surficial geology map units. Without a sufficient number of borings (generally >30 for each depth range of each geologic unit) the method may not reliable, and other approaches to mapping liquefaction hazard should be considered.

Step 2 - Ground shaking over the study area is characterized in Step 2. Areal distribution of ground shaking for assessing liquefaction factor of safety is represented by a liquefaction opportunity grid, consisting of magnitude-weighted peak ground acceleration for an alluvial site condition computed from a modified probabilistic seismic hazard analysis (PSHA). In the PSHA integration process, ground shaking hazard estimates are multiplied by the reciprocal of the duration weighting factor used in the updated simplified procedure for estimating liquefaction triggering potential (Idriss and Boulanger, 2008; Cetin et al., 2004; Youd et al., 2001). In this study, we used the simplified procedure of Youd and others (2001). Incorporating duration weighting into PSHA yields a shaking parameter that accounts for the effects of shaking duration on liquefaction triggering threshold probabilistically that can be used directly in the simplified procedure for calculating liquefaction factor of safety without additional scaling (Real et al., 2000). The resulting parameter is a duration-weighted peak ground acceleration, which we define as liquefaction opportunity.

Step 3 - Step three generates a liquefaction susceptibility grid by reclassifying the surficial geology map units based on a statistical analysis of geotechnical parameters and the computed liquefaction response strain-potential functions that result from the borehole log analysis of Step 1. To rank a geologic map unit’s susceptibility to liquefaction, we evaluate how samples of its soil column would respond to strong shaking when fully saturated. We hold depth-to-saturation and level of ground shaking constant while computing liquefaction potential of each geologic

unit, which allows comparisons to be made among soil column responses that reflect properties of the sediment only; that is, their propensity to liquefy. For comparison purposes we arbitrarily define liquefaction-deformation susceptibility to be the shear-strain potential for 100% saturation of the soil column subjected to a duration-weighted PGA of 0.4g from a M7.5 event. These values are well within the experimental and observational data upon which the simplified liquefaction assessment algorithms are based, while the specified PGA is high enough to test the stiffer saturated potentially-liquefiable sediment textures. That condition represents but one set of parameter combinations produced by the parametric modeling process of Step 1. The complete set of modeled responses from a boring log collectively defines the liquefaction potential of the represented soil column.

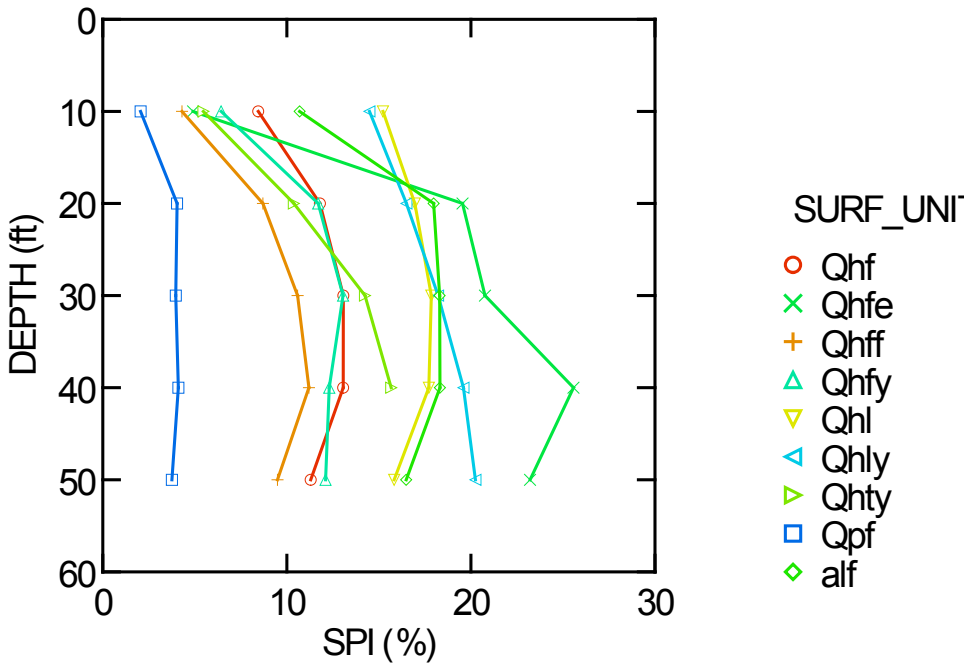

Figure 4. Examples of liquefaction response curves in terms of shear-strain potential index (SPI) for selected San Francisco Bay region Quaternary geologic map units (Real et al., 2008).

The first step in reclassification is to generate a median response for each geologic map unit by grouping the borehole data by the units they penetrate at the ground surface, and calculating a median shear-strain potential for each map unit. The process is optimized by calculating shear-strain potential as described in Step 1, only calculating median depth-interval displacements using all borings that penetrate completely through a given depth interval. Here the term “depth interval” means that portion of the soil column between two prescribed depths in the soil column. The procedure first takes shear-strain potential from the boring response matrix, and multiplies it by its corresponding depth range to yield displacement potential for each depth range, and then systematically differences them to yield displacement potential for each depth interval for each boring in the group. The median displacement over each depth interval is then calculated, using all borings for a given group that penetrate completely through the prescribed

interval. Summing each median depth-interval displacement from the ground surface to the prescribed depth range and dividing by that depth yields median shear-strain potential. This process is repeated for all prescribed depth ranges for each mapped alluvial unit.

Strain-depth curves (liquefaction response curves) of susceptibility shown in Figure 4 allow visual comparisons to be made among individual borehole logs and geologic map units that reflect only the sediment's capacity to liquefy and deform, independent of variations of depth to saturation or level of shaking. In the example in Figure 4, the older Pleistocene unit, Qpf, clearly shows the lowest deformation potential as expected. Geologic units are grouped (reclassified) into "susceptibility units" having similar propensity for deformation by comparing the liquefaction response curves and statistical distributions of soil properties. Classical statistical methods of multivariate analysis can be applied to grouped parameters assuming their distributions are normal. Most liquefaction-related parameter distributions show lognormal behavior for which it may be possible to convert to a normally distributed parameter by power-law transformation. Alternatively, non-parametric methods can be used to analyze the skewed data.

The third step is an interactive process that can result in splitting and lumping of surface geology map units based on similarity of geotechnical properties and liquefaction response computed from boring logs, supplemented by review of topography, air photos, and other remote sensing data commonly used for geologic mapping. The process constitutes a remapping of surface geology based on a sediment deposit's propensity to liquefy, and is most efficient when working with geologic maps that have already carefully differentiated Quaternary deposits based on their depositional environment and age. The result of Step 3 is a fourth grid over the region of interest that we define as liquefaction susceptibility grid that, when combined with the liquefaction opportunity, depth-to-saturation, and depth-to-liquefaction basement grids, is used to map hazard.

Step 4 - Step four creates a hazard potential matrix (HPM) that is used to integrate the above four spatial grids to produce derivative grids of spatially variable ground deformation potential and uncertainty (in this study first and third quartiles are used). The HPM is made by repeating the process of Step 3, only grouping by all borings falling within the newly-defined liquefaction susceptibility units. The result is a hazard potential matrix for each newly defined susceptibility unit in terms of median shear-strain potential and associated quartiles. The HPM is the key component of the proposed mapping process that allows the spatial variability of the independent variables to be accounted for and mapped independently using familiar surface and subsurface mapping methods. This is an improvement over approaches to liquefaction mapping that rely only on ranking surface geology, and using contact boundaries to define areas of hazard.

Step 5 - The final step in mapping liquefaction hazard is to combine the spatial grids using the hazard potential matrix to produce a grid of shear-strain potential over the area of interest. This can be accomplished on a raster GIS platform with grid analysis capability. Values in each cell of the four grids (liquefaction susceptibility, ground shaking, depth-to-liquefaction basement, and depth-to-saturation) can be re-coded to indices that correspond to the parameter ranges used to model the HPM. They then become an index to the HPM array in a lookup-table sense. For a

particular cell location, the indices for each parameter are read from the four grids and used to extract the value of shear-strain potential from the hazard potential matrix to produce the strain-potential grid. Additional grids can be produced in the same manner only extracting quartile values instead of the median to provide some uncertainty bounds on the mapping.

The final set of hazard grids is produced by a transformation from shear-strain potential to displacement potential and uncertainty. This is easily done by selecting the shear-strain potential grids and multiplying them by the depth-to-liquefaction basement grid to yield grids of DPI median displacement and quartiles.

1.6.2 Modifications to the "Proposed" Procedures

The above procedure is well suited for choosing whether or not to combine Quaternary geologic map units into discrete liquefaction deformation susceptibility units as described in step 3. The method is best applied where sediment lithology in the soil column is generally isotropic and homogenous, that is, there is little or no lateral continuity of stratigraphy, and where a maximum possible depth of liquefiable sediments can be identified. In the Delta region, the latter is problematic in that bedrock is very deep, and soft, liquefiable sediments sometimes extend beyond 50 feet. There is insufficient borehole data to identify and map the variability of a maximum depth to liquefaction. Thus, we arbitrarily chose a baseline elevation of -50 feet to compute the cumulative strain potential-depth curves for grouping of boreholes by surface geologic map unit boundaries, and statistically characterizing their median liquefaction response. The results are then used to group surface geologic map units into liquefaction-deformation susceptibility units having similar average liquefaction response as described above, recognizing statistical variability and testing for significant differences. We believe this approach is reasonable since liquefied layers at greater depths would be less likely to contribute significantly to surface manifestation of displacements. While used for defining susceptibility units, this procedure is NOT used to calculate estimated strains and residual displacements for characterizing hazard in terms of deformation potential.

The current research has resulted in enhancements to the "proposed" methodology for characterizing a liquefaction-deformation susceptibility unit's strain. Thickness and depth of discrete liquefiable units become independent variables in the response estimation process instead of the thickness of the entire soil column from ground surface to "liquefaction basement" (Step1 of Figure 2). Sub-surface stratigraphic analysis reveals a soft organics/peat layer, and a well defined sand layer that have continuity over much of the study area, thus providing valuable information on the spatial variation of liquefiable verses non-liquefiable unit thicknesses that can be taken into account when considering spatial coherency of displacement potential throughout the study area. The new approach has the potential to reduce epistemic uncertainty and significantly improve hazard estimation over the previous method when abundant, high-quality subsurface data are available to map the distribution of liquefiable material.

In this approach, instead of computing *cumulative* strain-depth functions based on liquefied layer thicknesses and using them to estimate total displacement to the "maximum depth of liquefaction" at a particular location, we compute strain-depth and displacement-depth *density* functions based on all of the individual *in situ* SPT sample measurements taken in potentially

liquefiable layers, grouping borehole data by surface liquefaction-susceptibility units and computing median strain over 5 foot depth intervals from the surface to 100 feet. Deformation at a grid cell is then estimated by integrating the strain-depth density functions over the limits defined by the top and bottom of the potentially-liquefiable sediment layers at a given grid cell location (Step 1 Figure 2).

To potentially reduce dispersion in the strain-density functions, we explore grouping of borehole data based on geologic map unit boundaries defined on 1) the current land surface, and 2) alternatively, on a geomorphic paleo-land surface. The latter has the potential to allow geomorphology to help guide interpretation of where silt- and sand-prone facies are likely to have been deposited, reducing the variance of liquefaction strain response functions thereby improving estimates of deformation potential. Our analysis, however, reveals that affects of present-day overburden would have to be removed, as was done for the levee boring logs, potentially introducing more error into the results. Furthermore, it will be seen that grouping of boring data according to the paleo-land surface geologic map units does not appear to reduce variability of computed strain response among units. Consequently, the second approach was eventually abandoned in this study, but may prove to be effective in other settings or with different data assemblages.

1.7 Principal Tasks

Work undertaken in this study is broken into 9 principal tasks shown in Table 1. Each task identifies the PI/organization leading the task. The remainder of the report is organized according to these tasks under two main sections, Analysis and Results, followed by Discussion and References.

Table 1. Principal tasks involved in preparing a liquefaction deformation potential map of the Sacramento-San Joaquin Delta study area.

Task No.	Description	Responsibility
1	Data collection and literature search	URS
2	Borehole Database development	CGS
3	Boring log interpretation	URS
4	Parametric modeling of liquefaction-induced strain	CGS
5	Subsurface stratigraphic analysis – boring log correlation	CGS
6	Preparation of paleo-land surface map	URS
7	Preparation of isopach maps	CGS
8	Liquefaction susceptibility analysis	CGS
9	Liquefaction potential analysis and hazard mapping	CGS

2 Analysis

2.1 Data Collected

Products made available from the CALFED ERP study include a valuable compilation of digital geologic mapping, vintage air photos and topographic maps, levee break database, and borehole location files in GIS format. These data were provided to us by the ERP contractor,

William Lettis and Associates (Hitchcock, personal communication). A comprehensive spreadsheet consisting of interpreted boring log data for nearly 2000 borings throughout the Delta was provided by URS Corporation. Original boring log data were acquired by a multitude of contractors over decades of levee investigations, and were made available by the California Department of Water Resources to the DRMS study. These data were analyzed by URS Corporation as part of the DRMS study. Of 1984 boreholes in the DRMS database, 942 are located in the vicinity of the study area, and of these 654 have penetration resistance measurements. Two of the study-area quadrangles (Antioch North and Brentwood) have too few borings to permit liquefaction hazard mapping and results extending into these quadrangles should be taken lightly.

2.2 Development of Database

CGS maintains an extensive borehole database management system (DBMS) in support of its seismic zonation work throughout the state. The liquefaction hazard assessment methods development in the PEER project and the current project serve to improve the tools used in the State-mandated hazard zoning, and the existing DBMS is used to manage the data in this study. In this study, boring logs summarized by URS for DRMS were imported into the DBMS. This required reformatting the data, and decisions on what parameter values to retain and which to re-compute. The majority of the borehole penetration test data was acquired over the years using a 1-inch sampler, which must be corrected to a 2-inch sampler performance in order to estimate a “standard” penetration test defined by ASTM standards. CGS applied a correct factor using the sampler tube inner and outer diameters and Burmister’s formula (1962) in order to approximate the standard 2-inch sampler used for a SPT measurement. Because the fundamental parameter used to derive strain is SPT expressed in blows per foot, and because the principal ancillary information contained in engineering boring logs is in the English system of units, the analysis and presentation in this research maintains this unit system.

Because of the limited funding in this project, no attempt was made to reinterpret the lithology logs, so the simplified interpretation from the URS database was assumed for the boring log lithology.

Because the objective of this study is to map liquefaction hazard over the study area using existing borehole data, and because nearly all borings were conducted through the Delta levees, adjustments had to be made to the data to make it representative of the adjacent land, without the influence of the levee soils (discussed in Section 2.4.1). Consequently, adjustments were made such that the top of the boring was made equal to the elevation of the levee toe.

2.3 Subsurface Stratigraphic Analysis

The Delta has been the subject of geologic and engineering studies for decades because of its important role in farming and conveyance of freshwater. Most recently, the aforementioned CALFED studies summarize the late Quaternary history of sedimentation, forced by rising sea levels at the Pleistocene-Holocene transition. Eustatic sea level fluctuations related to global glacial episodes resulted in the inter-fingering of bay estuarine deposits with terrestrial channel and floodplain deposits from the Sacramento, San Joaquin, and Mokelumne Rivers (Shlemon, 1971). During Pleistocene glaciations, wind-blown sand was swept from exposed terrestrial

sediments and deposited as dunes over much of the Delta region. The systematic warming trend at the onset of the Holocene was accompanied by glacial retreat, rising sea levels in the west, and the advance of tidal wetlands and marshes eastward into the Delta supporting the growth of reeds and tules that accumulated as peat deposits over millennia. Previous studies indicate a maximum accumulation of peat exceeding 60 feet near Sherman Island. ^{14}C dating of lowest (oldest) peat deposits yield ages of 6805 ±I 350 years b.p. in the Delta near Sherman Island (Atwater, 1982) compared to 7,360 ± 320 years b.p. in lowest peat deposits found in the San Francisco Bay (Storey, et al., 1966). The Pleistocene dune sands and river channel sands that are buried by the Holocene peat are deposits that are potentially liquefiable in the Delta.

Figure 5 is a geologic map of the study area as mapped by Atwater (1982). Atwater's mapping has been refined by Hitchcock and others (2005) by breaking out historical flood deposits and sediment from 19th century hydraulic mining activity in the Sierra Nevada Mountains. We chose not to use the revised geologic maps because the new units are not adequately sampled by the borehole data, and there would be no additional contribution to understanding liquefaction hazard using the methods employed in this study. Upon examination of Atwater's mapping, the central study area consists of two large outcroppings of the stratigraphic unit Qm2e (Upper Pleistocene wind-blown sand of the Modesto formation). This unit is surrounded by overlying Holocene peat and mud of tidal wetlands and waterways (Qpm formation) toward the north and east, and alluvial fan and terrace deposits (Qymc) from unglaciated drainage basins to the south. Attempts to use engineering characterization of surface stratigraphic units to extrapolate liquefaction susceptibility are problematic since much of the non-liquefiable deposits to the north overlie and conceal susceptible sands below. For this reason, a central strategy in this study focused on mapping the distribution of subsurface deposits over the study area, separating the liquefaction-prone units (sands and silts) from the non-liquefiable units (peat, soft organic silts and clays).

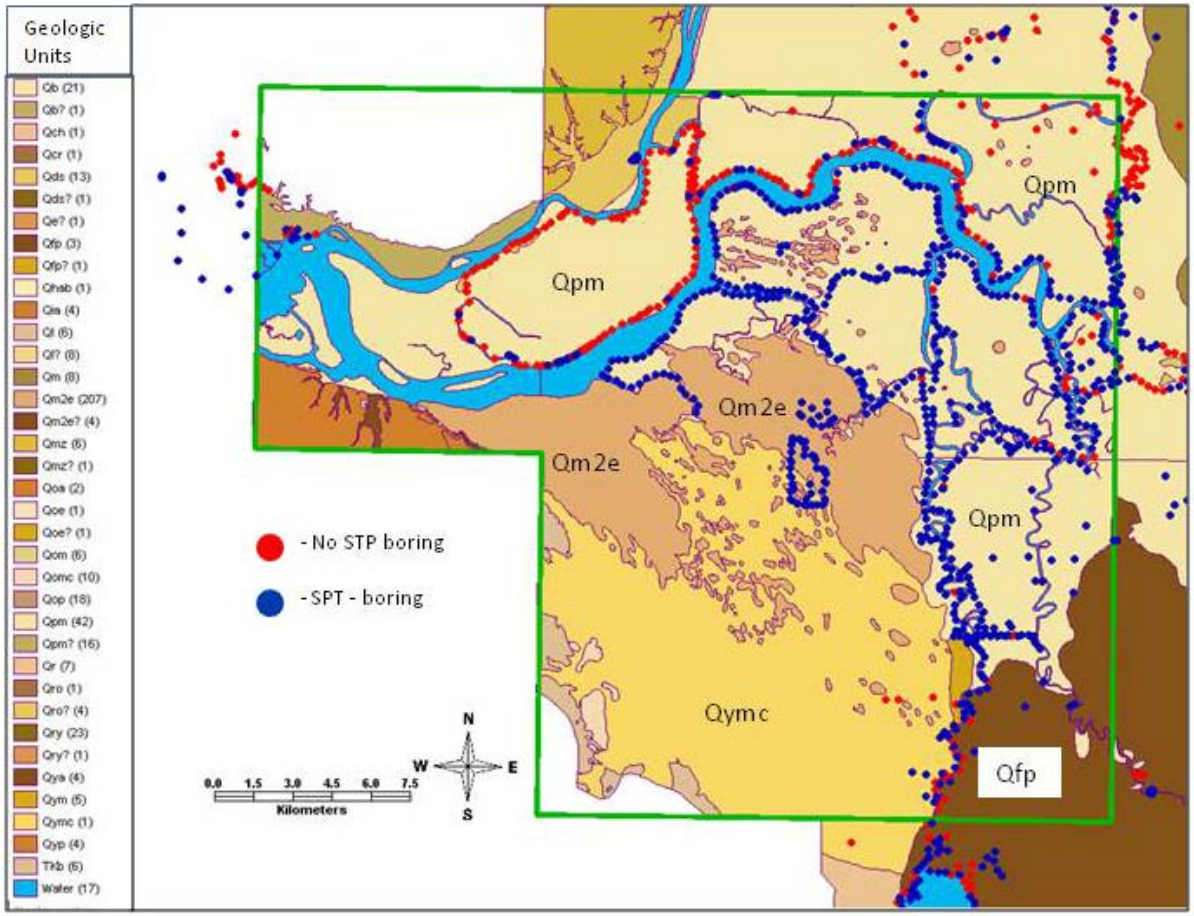

Figure 5. Geologic map of study area (after Atwater, 1982). Only the principal geologic units having boring log samples are labeled (Red dots are boreholes with no SPT; Blue dots are boreholes with SPT; Green line study area boundary).

2.3.1 Definition of Working Stratigraphic Units

We liberally define working stratigraphic units in an attempt to correlate the occurrence of sands throughout the study area. Because the scope of this study did not include reinterpreting the boring logs, we began with the lithology classes (Table 2) and boring log interpretations resulting from the previous DRMS, and define working stratigraphic units with the expectation of their being more contiguous throughout the study area. It is important to note that lithologic units have no implied sequence order in a boring column, and can occur randomly multiple times, whereas the stratigraphic working units are unique, and do have implied sequence order that imposes constraints in the process of boring log correlation. Of the four lithology types recognized in the DRMS study, SD (dune and channel sands) are clearly of *liquefiable* texture, while So (soft organics) and PT (peat) deposited in backwaters of lagoons, sloughs, and tidal marshlands of the Delta are *non-liquefiable* textures. All other soil types were lumped into Ot (other), which are predominantly floodplain deposits of silts and clays, and, although probably not strictly true, are considered to be predominantly non-liquefiable textures in this study.

Table 2. Reclassified/simplified sediment lithology from borehole logs (lithology after DMRS study, 2007; unit weights assigned in this study)

Lithology Designation	Description	Saturated Unit Weight (psf)
SD	Loose to dense silty sand	120
PT	Peat deposits	70
So	Soft organic fat clays and silt	99
Ot	Other undifferentiated soil lithology	149

In an attempt to track all sand deposits (SD lithology) while correlating logs, we initially define nine working stratigraphic units (Table 3). Peat and soft organics, which are almost always observed adjacent to one another, are combined into a single non-liquefiable unit. That combination of lithology is found to occasionally repeat in a soil column, separated by sands (SD) or silts/clays (Ot). We therefore define two working units consisting of these lithologies: Upper Peat and Organics and Lower Peat and Organics. In combination, these units were found to be continuous at depth over most of the study area as suggested by the surface geology. Occurrences of SD or Ot were kept independent as working stratigraphic units in an attempt to identify and track all potentially-liquefiable units over the study area independently. It was found that Ot is found to occur both above and below SD units preventing simple lateral correlation of units, so our stratigraphic sequence of Ot and SD units is arbitrary. Because the primary objective is to map thickness and depth of SD over the region, Ot occurrences are ignored in the correlation process. Assuming the only liquefiable material in the soil column is SD, as interpreted in the DRMS, variability of its thickness and depth controls the spatial variability of residual shear strain and displacements for the soil column as a whole.

Table 3. Working subsurface stratigraphic units defined in this study for correlation purposes (note colored rows correspond to color code of boring logs in Figure 13).

Initial Units	Final Units Correlated	Description
Levee	Upper deposits	Levees, interbedded sand, silts, clays
Upper Sand		
Upper Other	Peat and Organics	Peat and soft organics (fat clays, silty clays)
Upper Peat/Organics		
Middle Sand	Sand Unit	Sand, silty sands, minor other (includes Middle and Lower Sand)
Middle Other		
Lower Peat/Organics	Lower Deposits	Silty clays, clays, other.
Lower Sand		
Lower Other		

Upon conclusion of the subsurface stratigraphic correlation the nine initial working units dissolved into only four working units: Upper Deposits, Peat and Organics, Sand Unit, and Lower Deposits (Table 3). Thin, discontinuous lenses of varying sediment lithology were ignored and lumped into the thicker, more dominant and continuous units resulting in the "Final Units Correlated." The three key horizons mapped are: 1) the top of the Peat/Organics, 2) the bottom of the Sand Unit, and 3) the transition between these two units, which is the paleo-land surface upon which the peat and organics accumulated over the past ~7,000 years.

2.3.2 Preparation of Paleo-land Surface Map

To investigate the influence on estuarine deposition of the paleo-topography and paleo-geomorphic features that existed in the Delta prior to sea level rise about 8,000 to 9,000 years b.p., we prepared a map showing the base elevation of peat and soft organics. Plates 6.1 and 6.2 show the contours of this paleo-surface and the landward boundary of circa 1850 tidal wetlands.

To prepare the paleo-surface maps, we first compiled borehole data into a GIS database from two main sources: (1) the DRMS study; and, (2) Atwater (1982). This combined preliminary database included 3,117 boreholes, 1,610 of which were located in the five quadrangles that are the focus of this study. However, preliminary plots revealed several anomalies related to minimum, queried or alternative (i.e., multiple values given) elevations, mis-located boreholes, and some large discrepancies between adjacent holes (possibly due to logging/database errors or differences in geologic interpretation of the base of soft organics). Time constraints prevented checking original logs. Therefore, we removed all boreholes with alternative elevations (i.e., multiple elevations given), and those with queried depths that appeared anomalous (boreholes with queried depths that were highly discrepant from all nearby holes resulting in an isolated "bulls eye"). Boreholes with minimum depths that were less than the nearest adjacent holes also were removed. Next we performed a series of cluster analyses to identify adjacent boreholes with discrepant depths that appear highly suspect (specifically, holes located within 15 m of each other and having depth differences ≥ 5m). Some of these appeared

to be due to mis-located boreholes, resulting in erroneous top-of-hole elevations, and these were removed. For most holes, specific reasons for the discrepancies could not be identified but often obvious anomalies compared to all surrounding holes could be identified and these were removed. Finally, because Atwater's (1982) study had a geologic focus and the DRMS study a geotechnical focus, for the purposes of our map we judge the geologic interpretations of the former to be more reliable than the latter. Therefore, we reviewed individual DRMS boreholes that were located within 15 m of an Atwater (1982) borehole if the difference in base of peat elevation was ≥ 5 m. An additional filter was applied by removing all DRMS boreholes within 100 m of an Atwater borehole if the difference to the basal peat was likewise ≥ 5 m. Thus the total number of boreholes used in contouring the final map was 2,231, with1,092 from Atwater (1982) and 1,239 from the DRMS study. 1,294 of these were located within the five-quadrangle focus area of this study.

In addition to the boreholes, we also used Atwater's (1982) 1850 "tideline" ("landward margin of tidal wetland at low river stages circa 1850"). Shown on Plate 6.1 and Plate 6.2, this line generally marks the extent of estuarine-dominated deposition of peat and soft organics in the Delta and therefore should roughly correspond to a 0 m elevation. However, because Atwater's (1982) elevations were relative to NGVD29, and our map is relative to NAVD88, points on his 1850 tideline roughly correspond to an elevation of about 0.7 m or 2.3 ft above sea level on our map.

We used the program, "Topo to Raster" in the ArcGIS software family (ESRI), to contour the surface of the base of peat elevation, which uses a spline function to interpolate between points. The splining function depends on both the cell size and discrete error factor used in the interpolation. The latter can vary from 0.5 to 2, and is a measure of the elasticity or stiffness of the surface, with larger values resulting in smoother surfaces. For our final maps, we used a cell size of 200 m, and a discrete error factor of 2 to produce a more smoothed surface because it appeared to be more geologically reasonable and consistent with the scale of this study than versions with smaller cell sizes.

Based on this analysis, we observe that:

- Since the 1880's, subsidence has occurred at various rates in the Delta, with as much as 8 m in some locations. This subsidence is primarily due to oxidation of organics related to agricultural practices and our map does not account for (remove) these because they are presumably occurring above the paleo-land surface.
- Our results are generally consistent with previous studies (Shlemon, 1971; Atwater, 1982) but have more detail. In particular, four major geomorphic features dominantly influenced estuarine deposition in the Delta. These include: paleo-channels of the San Joaquin River in the south, paleochannels of the Sacramento River in the north, Mokelumne alluvial fan deposits to the west, and a north-northwest-trending dune field located east and southeast of Sherman Island.
- Maximum depth of peat exceeds 20 m and is located where channels of the Sacramento and San Joaquin Rivers converge around Sherman Island. The paleochannels of these north-south trending major river systems, and to a lesser extent the Mokelumne River,

apparently formed accommodation space for thicker estuarine deposition. In contrast, coalescing Pleistocene Mokelumne alluvial fan deposits at the eastern margin of the Delta generally limited the east extent of Holocene estuarine deposition, resulting in an overall north-south elongated estuarine basin.

- Just east and southeast of the maximum basin depth near Sherman Island was a Pleistocene dune field that formed a paleo-topographic high, where estuarine deposition was limited to non-existent.

2.4 Boring Log Deformation Analysis

2.4.1 Removal of Levee Overburden

Nearly all of the geotechnical boreholes in the study area have been drilled through levees. Because the objective of this research is to assess the liquefaction hazard of native sediment leave foundation deposits, when modeling liquefaction response, we adjusted the boring logs to account for the absence of levee material overlying the natural deposits when estimating liquefaction response over the region as a whole. First, the penetration resistance measurements were corrected in the standard fashion using the original, unaltered logs to produce fines corrected standard penetration resistance at 1 atmosphere. That required correcting field measurements from a one-inch sampler to a standard two-inch sampler, and specifying unit weights for USCS lithology calls for levee material and for the native soils beneath them. After calculating $N_{1,60,cs}$ from the *in situ* measurements, an "adjusted" set of boring logs were made by a) making elevation of the top of the boring log equal to the toe of the levee, and 2) removing the levee overburden material above that elevation as if it did not exist. The revised boring logs were then analyzed for liquefaction potential using the corrected penetration measurements and 100% saturation of the revised sediment column representing only the natural deposits, for specified levels of shaking.

2.4.2 Parametric Modeling of Borehole Response

Of the nearly 2000 boring logs available in the URS Delta database 942 are located within the 5-quadrangle study area boundaries (Figure 5). Of these, 654 boreholes have SPT data, with results of 3,702 in situ measurements taken at various depths ranging from less than 1 foot to in excess of 100 feet. As described in the Section 1.6.1, each boring log is evaluated for liquefaction triggering using the simplified method (Youd and others, 2001). After applying all corrections to yield $N_{1,60,cs}$, we compute SPT sample strains and cumulative residual strains to a depth of 50 feet by subjecting each boring log profile to a spatially-uniform 0.4 pga from a M7.5 earthquake assuming 100% saturation of the soil column (calibration conditions) as described under Methodology. Thus, differences in the strain values from boring to boring should only reflect differences in sediment properties, allowing comparisons of liquefaction susceptibility to be made without the influence of varying shaking intensity or degree of saturation.

In addition to the susceptibility "calibration" run at 0.4g, we also model each borehole liquefaction residual strain/displacement response for 0.2 and 0.3 duration-weighted PGA, which represents the range of shaking in the study area for a 10% in 50-year exceedance probability for alluvium conditions. We then group all borehole response curves by the

liquefaction-susceptibility units they penetrate, and compute median and quartile response curves.

2.4.2.1 Sample Analysis

Figure 6 shows the frequency distribution of $N_{1,60,cs}$ from 3,702 SPT sample measurements at a range of depths below the ground surface, which clearly indicates a skewed lognormal-like distribution, as expected for the standard penetration test. Figure 7 shows superimposed on the same data a continuous Lognormal (a) and Weibull (b) distribution. The Weibull distribution, often used in failure analysis to characterize strength parameters, shows a better fit to the SPT parameter. Figure 8 shows frequency distributions for computed strains, which are also skewed. Given the skewed distributions of these parameters, liquefaction-deformation hazard estimates and uncertainty are expressed as the median and quartiles respectively.

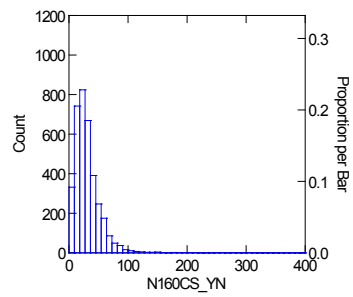

Figure 6. Histogram of 3,702 standard penetration tests in study area showing a skewed lognormal-like distribution.

(a) (b)

Figure 7. Lognormal (a) and Weibull (b) distributions fit to the standard penetration test data.

(a) (b)

Figure 8. Histograms of 3,702 sample estimates of strain: a) shear and b) volumetric reconsolidation. These parameters have a highly skewed distribution, which restricts the statistical methods that can be used to test for significance in the analysis of strain and deformation to non-parametric tests.

To illustrate the method used to calculate deformation indices (displacement potential) we take all strain calculations for SPT samples in liquefiable textures (SD unit) throughout the study area and produce a strain-density vs. depth curve (generalized response function for illustration only) for the calibration conditions of 100% saturation, and 0.4g from a M7.5 earthquake (Figure 9). Hazard Potential Curves similar to this are computed for the alternative shaking levels and borehole log groupings for defined liquefaction-deformation susceptibility units as described previously. Displacement potential is calculated by integrating the curve over the depth range (thickness) defined by the top and bottom elevation of liquefiable sand layers.

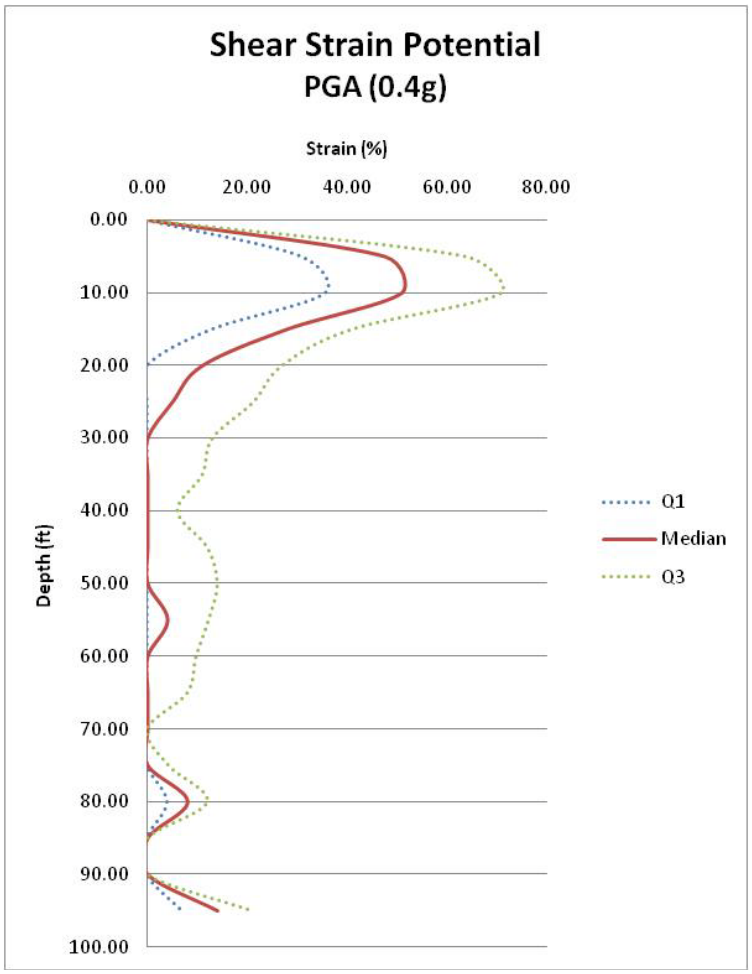

Figure 9. Shown is the median and first and third quartiles for shear-strain density vs. depth computed for all 3,702 SPT measurements in potentially liquefiable materials throughout the study area (for illustration only; no grouping of measurements by geologic units has been done).

2.4.2.2 Layer Analysis

We performed a “layer” analysis of the borehole penetration data in order to analyze the liquefaction susceptibility of the Delta sediments as described in Section 1.6.1. In the layer

analysis for a borehole, we average all of the individual sample SPT measurements taken in a discrete lithologic layer of liquefiable texture and assign the value to a depth defined by the middle of the layer. In computing the cumulative strain to a given depth, we use equation 1 presented in Section 1.6.1, summing to a prescribed depth at 10 ft increments each liquefied layer's contribution to displacement and dividing by the depth to yield average strain. Grouping of borehole data is done as described in the previous section, and median and quartile *cumulative* strains are computed. This approach results in a generalized set of point values of average strain to depth in 10 foot intervals. The curves can be displayed as a step over each depth interval, or simply as straight-line segments connecting each depth-strain data pair. We have arbitrarily chosen the latter, as no further computations are made from these response curves. They serve only to represent a "signature" for each boring log, or group of borings that sample a surface area defined by geologic unit boundaries, or other unit boundaries interpreted from geomorphology and geology, etc. The next section discusses the comparison of the various "signatures" from which the liquefaction-deformation susceptibility units are derived.

2.5 Liquefaction Susceptibility

2.5.1 Existing Surface Geology

To assess the susceptibility of Delta sediments, we computed liquefaction deformation response curves (cumulative strain-depth curves at 0.4g) to "calibrate" the surface geologic map units defined by Atwater. Only four geologic units have sufficient borehole data for the calculation: Qymc, Qpf, Qm2e, and Qpm (Figure 10). The response curves for Qymc (blue dashed) and Qpf (red dashed) are very similar, while those of Qm2e and Qpm are distinctly different. High strain (displacement) potential is observed for the thick eolian sand deposits (Qm2e), whereas the lowest strain (displacement) potential is observed for the peat and soft organic deposits (Qpm). The latter geologic unit is underlain by Pleistocene eolian sands (Qm2e) at depths ranging from near-surface near the Qm2e contact boundary to in excess of 60 feet near Sherman Island (see Figure 15). Thus, although representing predominantly non-liquefiable material, the low strain values for this unit reflects the limited occurrence of these sands at depths of concern for liquefaction. The orange dashed line in Figure 10 represents the combined dataset for Qymc and Qpf, which can be lumped together as a single liquefaction-deformation susceptibility unit. Consequently, for the analysis based on the existing surface geologic mapping, three sets of strain-density response curves are computed and used to estimate deformation potential over the study area as Alternative-A.

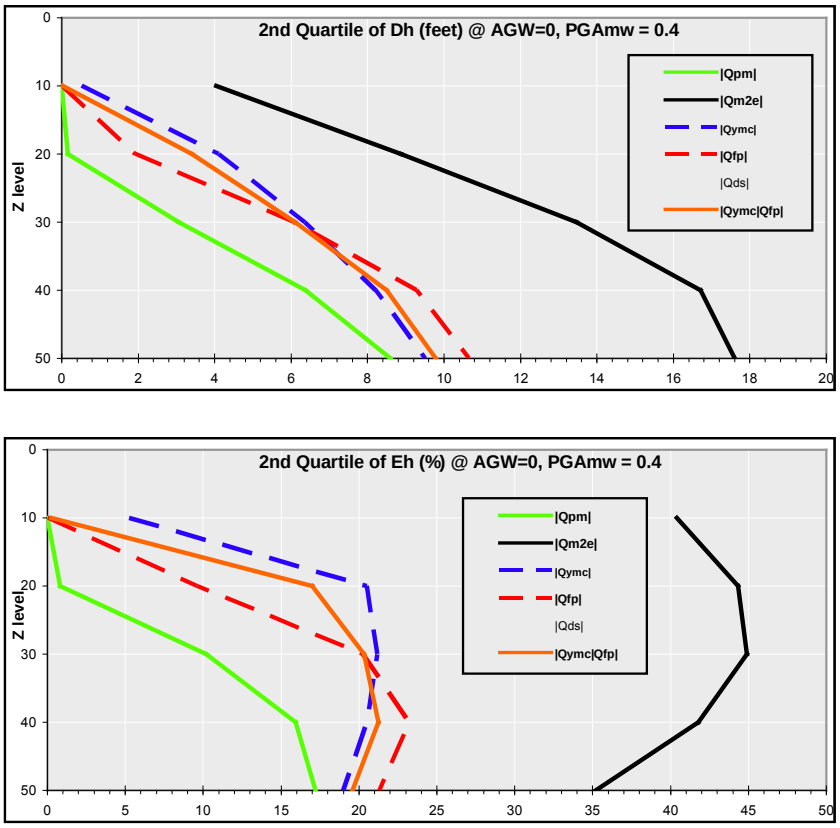

Figure 10. Cumulative-displacement and shear-strain “signatures” for borehole groupings by surface geologic map units after Atwater (1982). Dashed curves (Qymc and Qfp) are similar, and their combined data set is shown as the solid orange curve (upper figure: displacement; lower figure: shear strain).

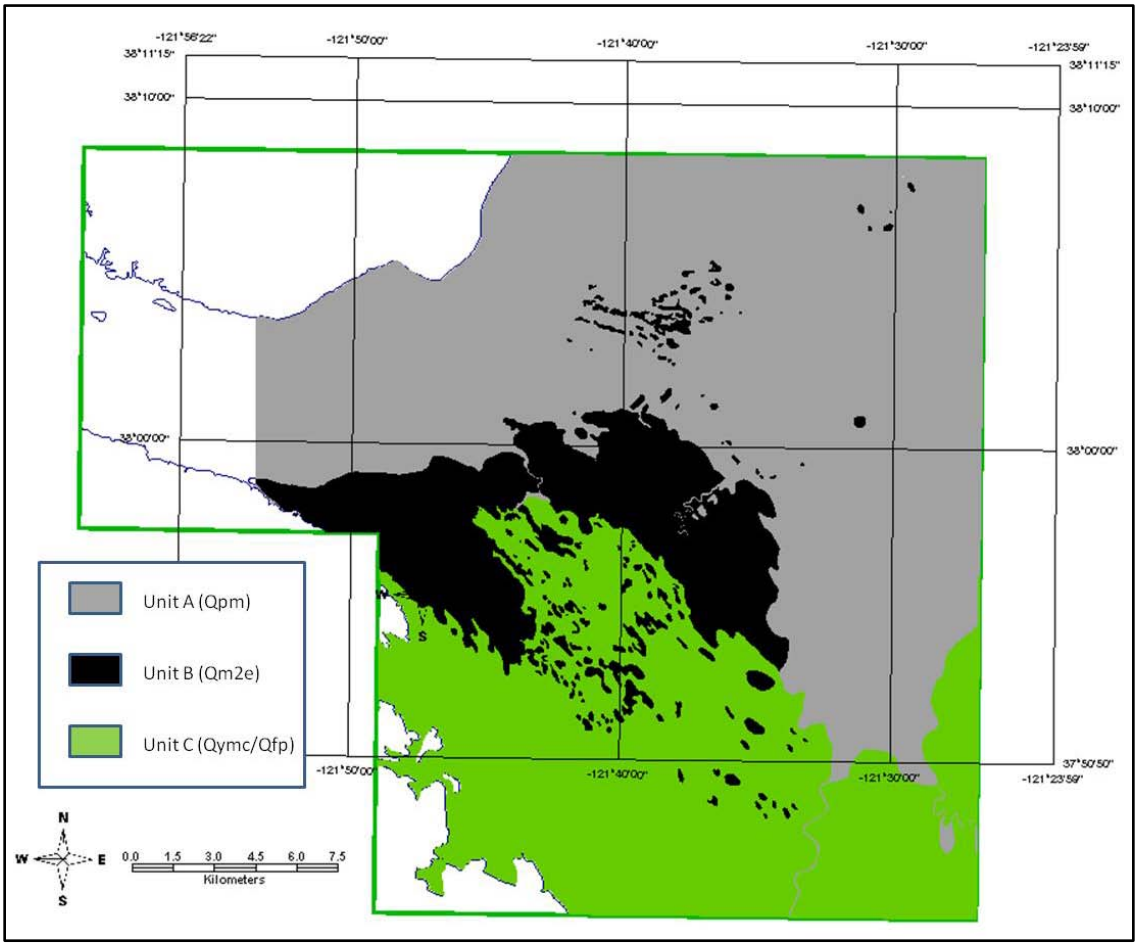

Figure 11. Liquefaction-deformation susceptibility map reflecting the grouping of present-day surface geologic units (Atwater, 1982) resulting from this analysis. We converted this layer to grid format and use it to select the set of liquefaction response curves to use in computing deformation potential at a given cell location.

2.5.2 Paleo-Land Surface Geology

Alternative-B analysis was conducted in a similar manner as the preceding only evaluating the geologic units mapped on the ~7,000 b.p. (pre-peat formation) paleo-land surface. As evident in a comparison between Figures 11 and 13, geologic units and boundaries on that surface are significantly different. There is no peat-soft organics unit (Qpm), the eolian sand unit (Qm2e) extends farther north where it is now overlain by the present-day Qpm unit, and present-day Holocene fluvial floodplain deposits Qfp have been divided into two units separating deposits of the Sacramento River (Qfp1) and the Mokelumne River (Qfp2). The cumulative-strain and displacement index response curves calculated for these units are shown in Figure 12.

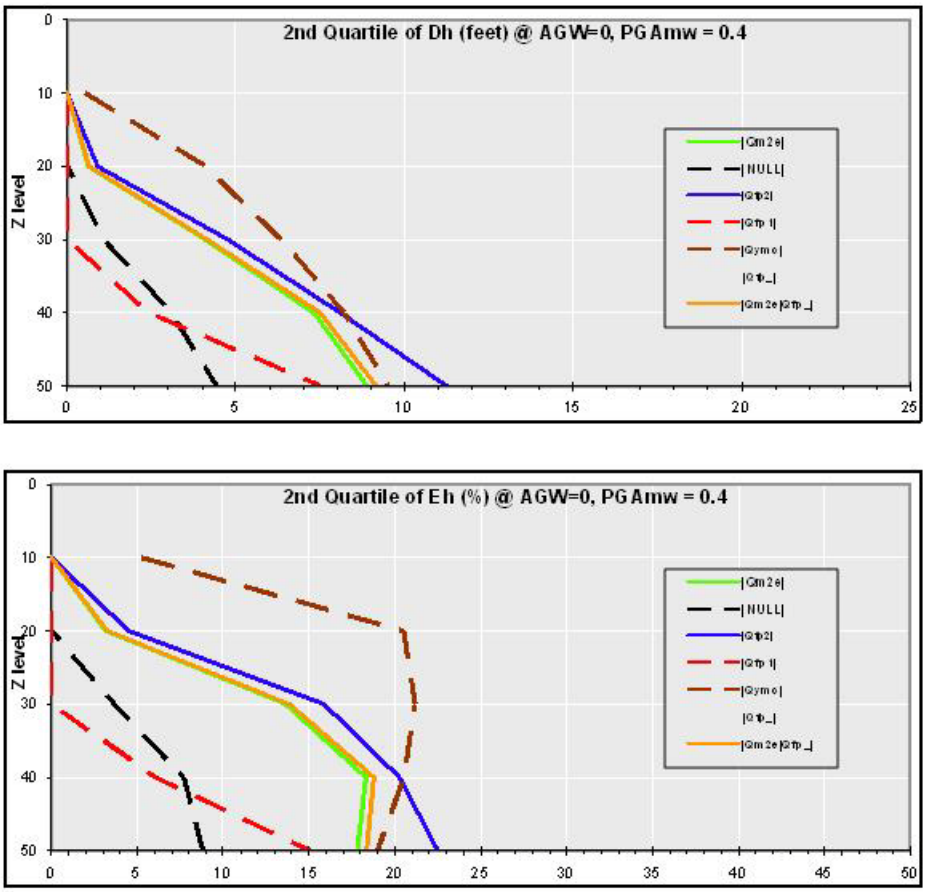

Figure 12. Cumulative-displacement and shear-strain "signatures" for borehole groupings by paleo-land surface geologic units defined in this study. Blue and Green curves (Qm2e and Qfp2) are similar, and their combined data set is shown as the solid orange curve. The black dashed curve represents boring logs that fall outside of the paleo-surface map area (upper figure: displacement; lower figure: shear strain).

When comparing these results with those of the previous section based on current geologic mapping, the most dramatic differences arise from the exclusion of geologic unit Qpm (peat and soft organics). By definition, the paleo-land surface predates deposition of Qpm, which is non-liquefiable sediment, and hence, contributes no residual liquefaction strain. Grouping borings by boundaries of the paleo-geologic map for each surface geologic unit, Qm2e (eolian sands), Qfp1, and Qfp2, which all extend northward underlying the present Qpm, has the effect of reducing their overall cumulative strain estimates (compare Figures 10 and 12). That is because boring logs are included in the averaging process that contain a significant amount of non-liquefiable peat and muds, and have correspondingly lower cumulative strain-depth curves. Unit Qymc is unaffected by the absence of unit Qpm, and consequently the cumulative strain-depth curve is identical to that computed for the existing surface geology (Figures 11 and 13). To account for the effect of overburden, and develop meaningful strain-depth density curves for estimating displacements based on the paleo-land surface geologic map, would have required adjusting all boring log strain calculations by effectively removing the Qpm overburden. This process would have been analogous to what was done for estimating strain response of the native sediments by removal of levee overburden as described in Section 2.4.1. It is likely that more error would have been introduced in the hazard estimate using this procedure, so we decided to conclude Alternative B analysis, and limit utility of the paleo-land surface to helping assess interpretation of subsurface stratigraphy.

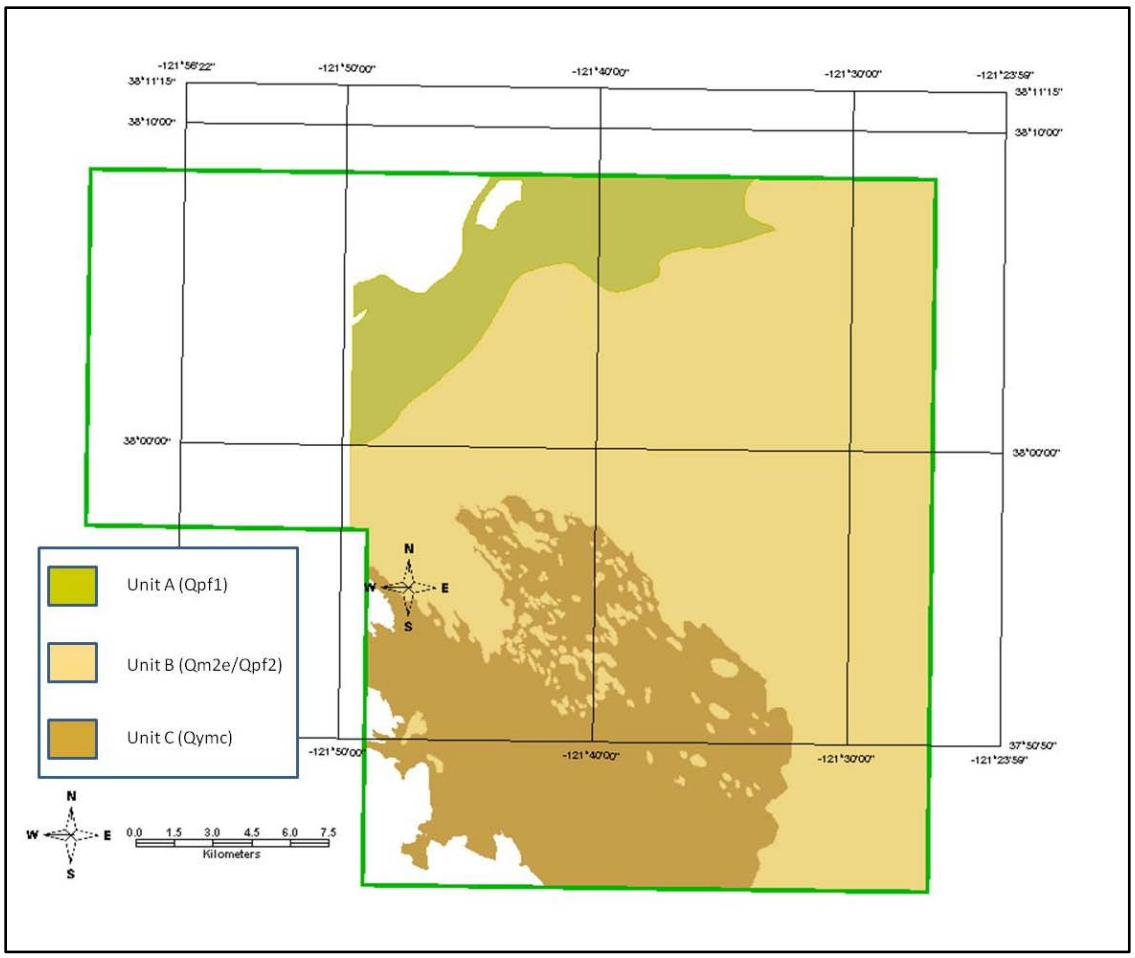

Figure 13. Liquefaction-deformation susceptibility map reflecting the grouping of paleo-land surface geologic units defined in this study (alternative B). We converted this layer to grid format and use it to select the set of liquefaction response curves for use in computing deformation potential at a given cell location.

2.6 Ground Shaking

2.6.1 Peak Ground Acceleration

Earthquake shaking intensity used in the study is based on probabilistic seismic hazard analysis using the 2002 joint USGS-CGS model for California (Cao et al., 2003; Frankel et al., 2002). Ground motion was expressed in terms of peak horizontal acceleration having a10% probability of exceedance in 50-yr, adjusted for alluvium site conditions using the NEHRP soil factors (FEMA, 1994). This is the same ground shaking input used in the hazard evaluation for delineation of seismic hazard zones by CGS.

2.6.2 Liquefaction Opportunity

When analyzing liquefaction potential, induced cyclic stress ratio is estimated using duration-weighted peak horizontal ground acceleration. We followed the procedure described previously in Step 2 of Section 1.6.1. In this manner differences in the contributions to induced cyclic stresses from large distant events verses small local events are recognized and incorporated probabilistically into the resulting "weighted", or "pseudo" acceleration, such that the additional cycles of high ground motion from large distant events is properly accounted for. The duration-weighted PGA varies from .2g to .3g over the study area, as shown in Figure 14.

3 Results

3.1 Principal Subsurface Units

Figure 15 is a set of 3-D views of boring lithology logs over the entire study area. Continuity of peat and soft organic deposits (shown as dark brown) and underlying sands (shown in yellow) is clearly indicated over much of the area. These sands are interpreted to be contiguous with surface outcrops of Pleistocene eolian sands (Qm2e) in the southern portion of the study area (Figures 5 and 16). These two units are key to the results of this study, because stratigraphic correlation of their interface (bottom of peat/top of sand) allowed mapping of the early Holocene (~7,000 BP) paleo-land surface and thickness of potentially liquefiable sands.

For purposes of borehole log correlation the study area was divided into 6 overlapping sub-regions as shown in Figure 16. Maps corresponding to each sub-region showing locations of boreholes and section lines are hyperlinked to this figure, and can be viewed by clicking on the subarea name box to bring up a profile index map, and clicking again on each profile name box to view the corresponding correlation panel (68 panels in all). Several hundred boring logs were correlated, working within each overlapping sub-region. The borehole database contains no boring logs for most of sub-regions 1 and 5. Lacking the critical data for stratigraphic correlation, most of this area is excluded from the final liquefaction hazard maps.

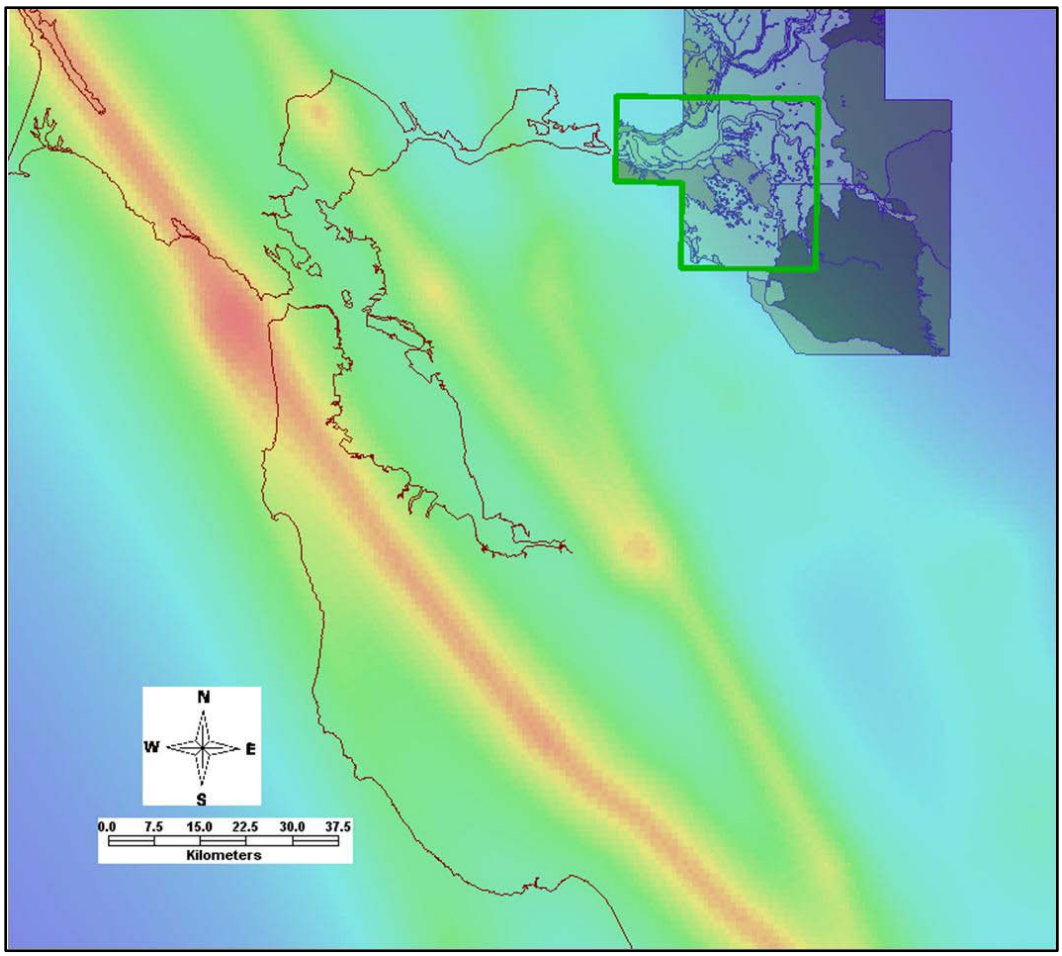

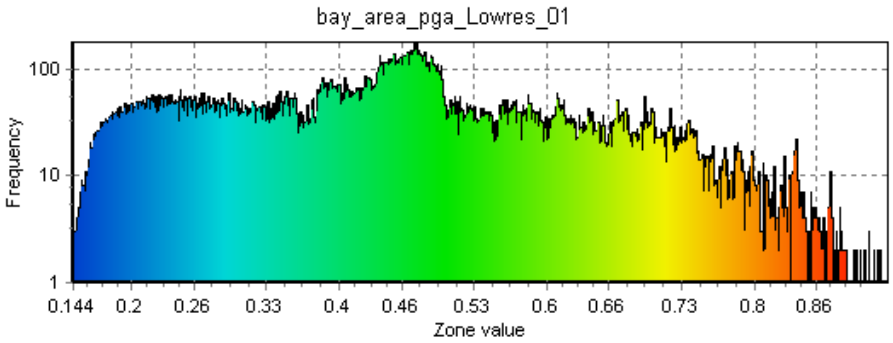

Figure 14. Duration-weighted alluvium peak horizontal ground acceleration (g) having a 10% probability of exceedance in 50 years (CGS, 2002). Bright bands correspond to the San Andreas-Hayward-Calaveras fault system. Delta study area is located in upper right, where shaking varies between .2-.3g. The figure below is a color-legend frequency histogram of the number of pixels having the corresponding zone value This style of legend accompanies other raster-type map figures in this report where the zone value represents the principal parameter portrayed on the map (e.g. PGA on this map).

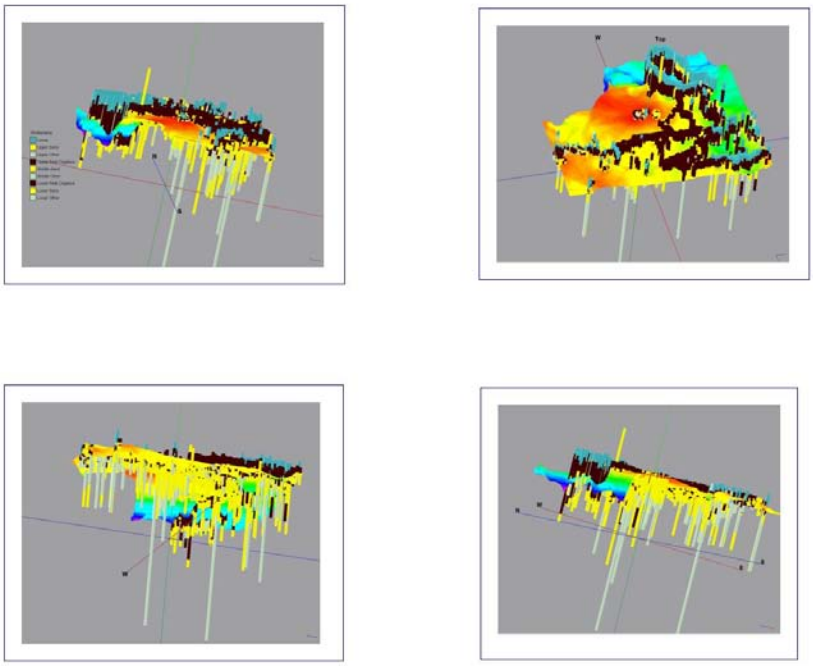

Figure 15. Four different views of the lithology logs from all borings used in study. Surface shown is bottom of peat-organics layer, which represents the paleo-land surface upon which the peat has formed from early Holocene to present. Note upper left and bottom right views show deep accumulation of peat to the west (dark brown) and all reveal extensive sands beneath the peat (yellow). (click on each figure to view enlarged image).

3.1.1 Non-liquefiable Units

Peat and soft organics (Qpm) are predominantly non-liquefiable sediments that range in thickness from more than 60 feet in the northwest portion of the study area near Sherman Island, thinning toward the south to zero thickness in the central study area as shown in the 3-D boring log display (Figure 15) and total peat thickness map (Figure 17). Also identified in logs, but too discontinuous to track are clays and silts. These deposits occur at the surface, within the thicker peat layers, and below, and are highly discontinuous except in the deeper section in the southeast portion of the study area. Although examination of original boring logs suggest sediments identified in the URS boring database as OT may contain some potentially liquefiable silts, their occurrence is very intermittent and unpredictable. Most of the OT-classified sediments are of fine, non-liquefiable textures. Therefore, we consider the entire lithologic unit OT to be non-liquefiable when mapping the hazard.

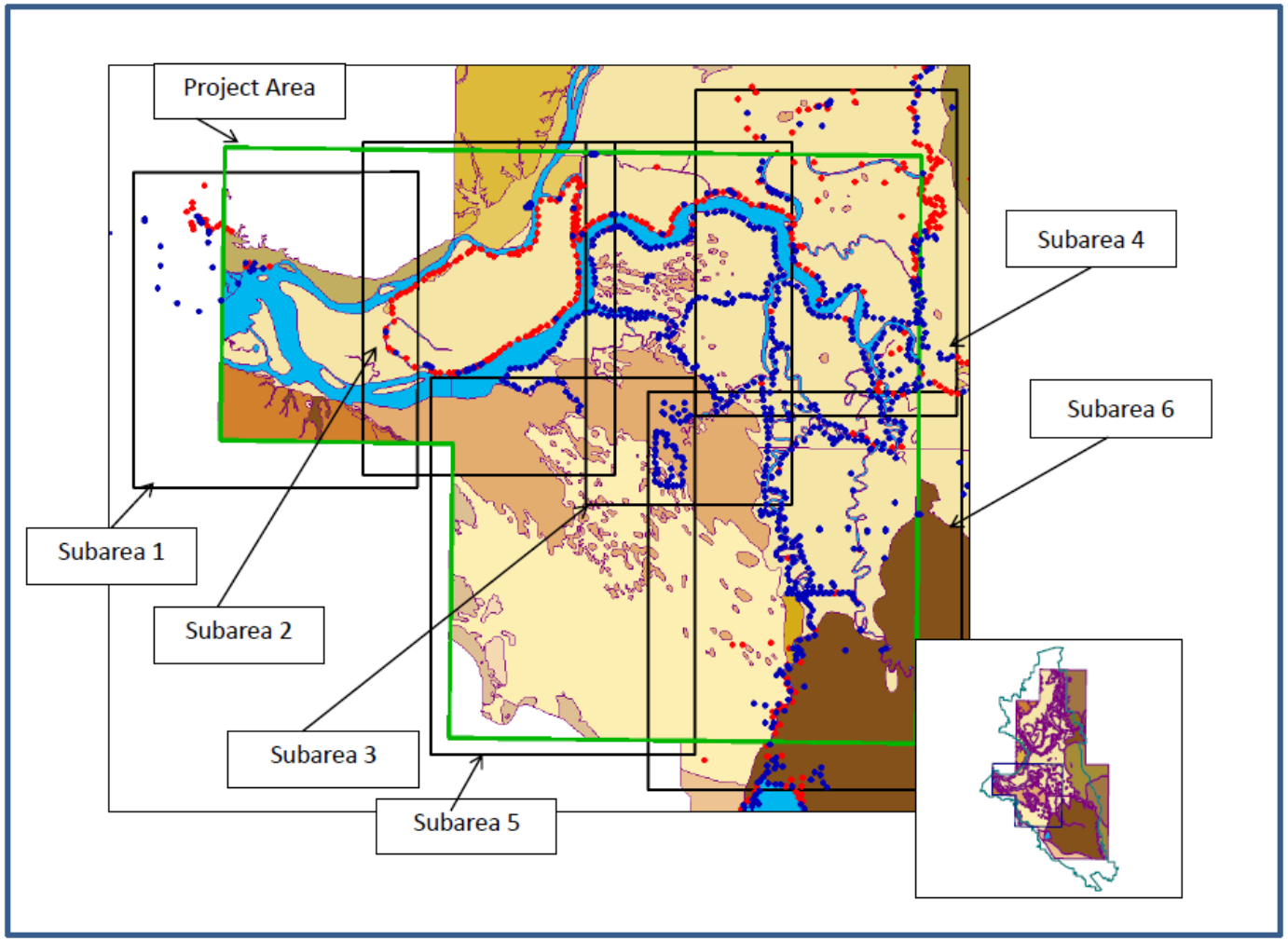

Figure 16. Subareas defined for stratigraphic correlation of borehole logs. Only subareas 2, 3, 4 and 6 have sufficient data for analysis. Boreholes are color-coded as follows: Red dots are boreholes with no SPT; Blue dots are boreholes with SPT. Background geology is after Atwater (1982). (Note: click on Subarea names to see boring log profile map> Then click on profile names on profile map to see the corresponding correlation panel – 68 panels in all. Panel colors correspond to stratigraphic units in Table 3 and Figure 13).

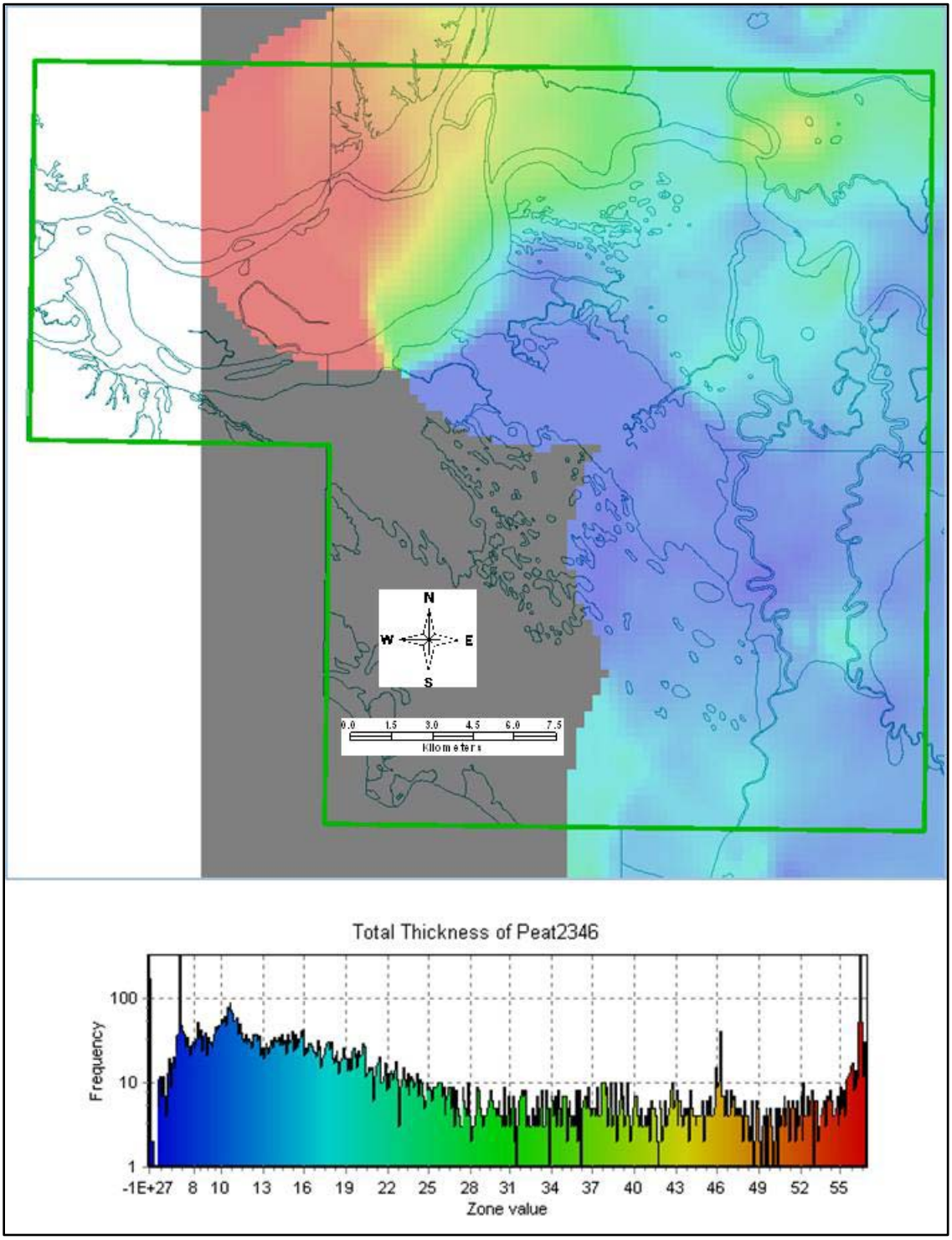

Figure 17. Isopach map of Peat-Organics working unit over study area. The unit thickness ranges from over 55 feet in the northwest near Sherman Island to zero in the southeast. The area to the southwest (gray) is void of data and has little, if any, peat. The legend is a frequency histogram as described in the caption for Figure 14 (zone value is unit thickness in feet).

3.1.2 Liquefiable Units

Exposed at the surface in the central study area, and beneath the peat/organic sediments, lie thick deposits of late Pleistocene age dune sands, which form the land surface upon which the peat beds formed (Figure 15). Fluvial sands also were deposited upon this surface from active channels of the San Joaquin, Mokelumne and Sacramento rivers, but it is not possible to use multi-log correlation panels to determine the lateral extent and thickness of these deposits away from their current channels because nearly all of the boreholes are confined to the current levee system. No attempt was made to differentiate between these deposits at depth, and thus we defined and mapped a single sand unit over most of the study area. The occurrences of sands above or intermixed within the peat units is too discontinuous to correlate between boring logs, and is not considered in the analysis. While in some cases they may be locally thick, and have an important bearing on liquefaction potential, that level of detail is beyond the scope of this study and scale of mapping supported by the areal density of borehole data available.

Figure 18 shows an isopach of the principal sand layer that was correlated over the study area. The thickest part of the sand unit lies in the central portion of the study area (Webb Tract, Franks Tract, Branford Island, Bethal Island, Jersey Island, Hotchkiss Tract, and Holland Tract), thinning rapidly toward the west and northwest, and less rapidly toward the south and the east (Figure 19). As previously mentioned, although the isopach map shows substantial thickness of sands in the southwest portion of the study area, borehole data are lacking so caution is advised when interpreting the results of stratigraphic interpolation/extrapolation.

3.2 Liquefaction Deformation Potential

3.2.1 Liquefaction Deformation Potential Functions

Figures 20 and 21 are the median liquefaction shear-strain density curves for the three liquefaction-deformation susceptibility units (Figure 11), showing the first and third quartiles (edges of box), mean (red dot), median (blue line in box), and the data range as whisker bars. There are two sets corresponding to input duration-weighted peak alluvial ground accelerations 0.2g and 0.3g, which covers the range of shaking intensity estimated for the study area.

We checked each susceptibility unit for statistical significance using the Kruskal-Wallis one-way analysis of variance, or H-test. As noted in Section 2.4.2.1 the distribution of borehole strain estimates is highly skewed, and the H-test is a non-parametric test that can be used for making multiple comparisons of non-gaussian data. Based on over 3,000 SPT measurements, the H-test indicates that there are real differences in strain-density vs. depth curves for the three susceptibility units. To further focus on curve significance, we applied the H-test for 5 foot depth intervals. Results for comparison of the three susceptibility units for both shear strain and volumetric reconsolidation strain for duration-weighted peak ground accelerations of 0.2g and 0.3g are shown in Table 4 and Figures 22-23. Only the depth range from 0-30 feet (indicated by yellow band) shows statistically significant differences in strain for both shear and volumetric reconsolidation strains, as the other depth intervals have too few sample measurements for significance.

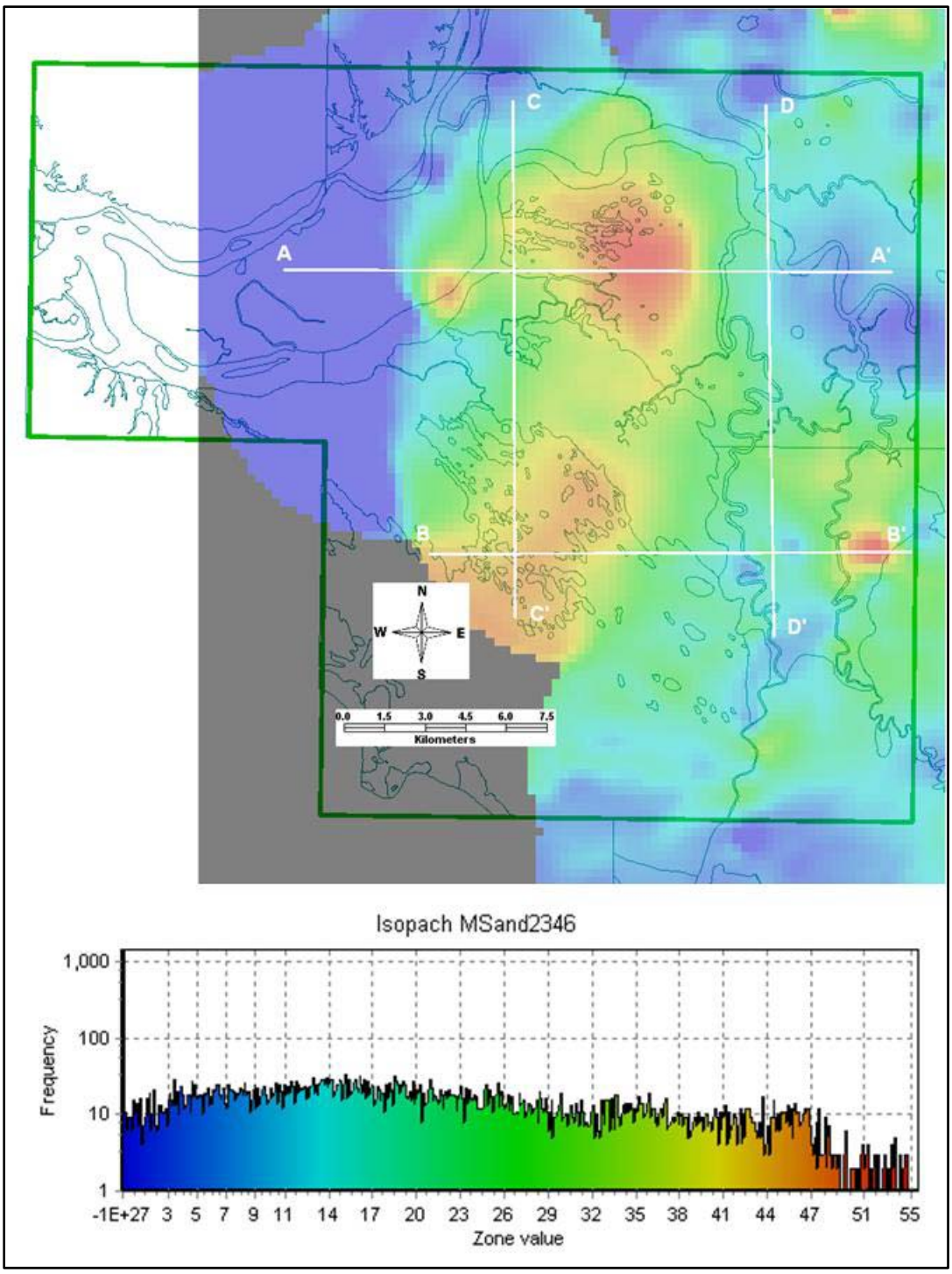

Figure 18. Isopach map of the Sand unit over the study area. The thickness ranges about 40-50 feet in the central area to zero toward the west, where the overlying peat-organics is the thickest. Also shown are profile lines corresponding to the cross-sections shown in Figure 19. The legend is a frequency histogram as described in the caption for Figure 14 (zone value is unit thickness in feet).

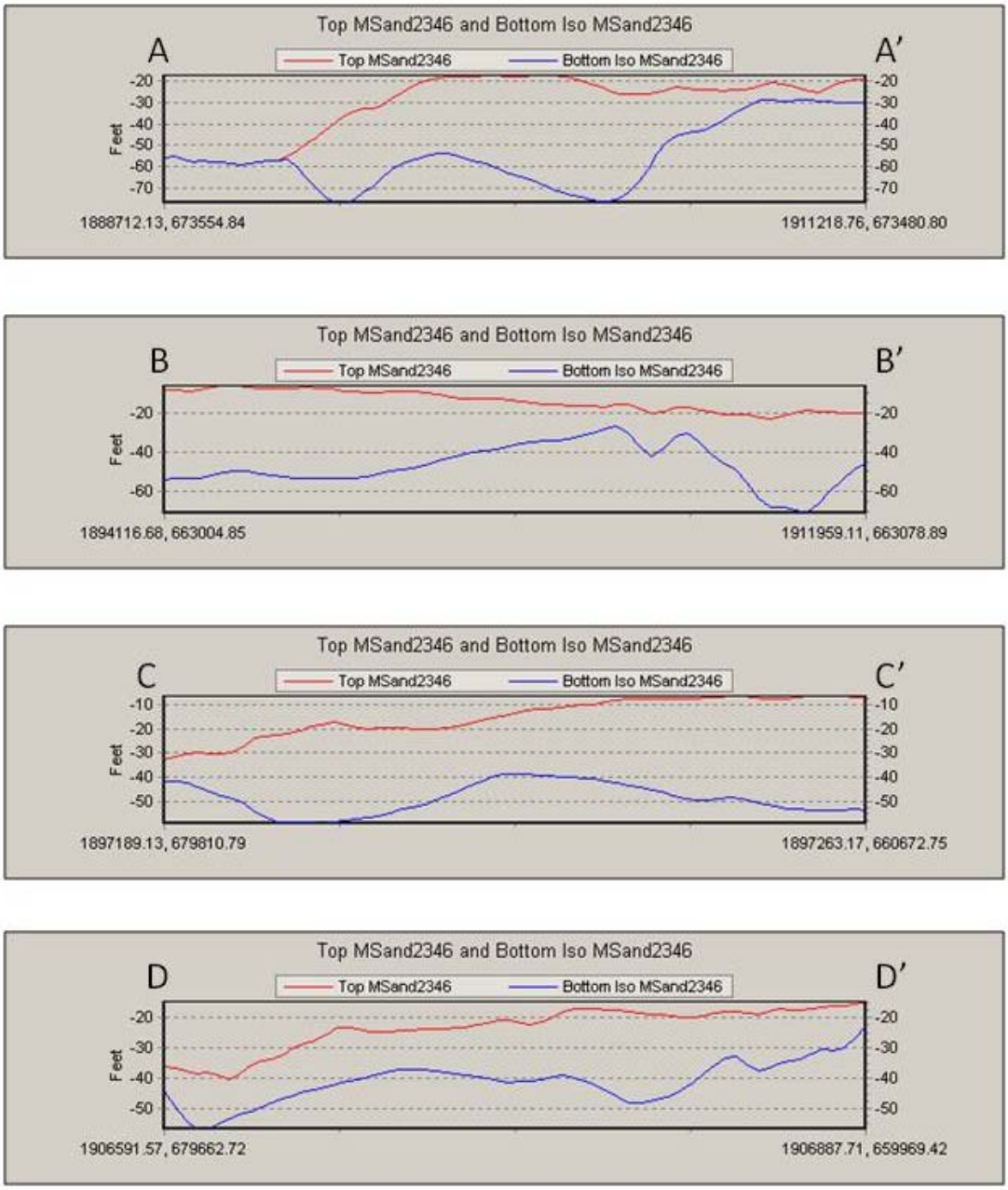

Figure 19. Cross-sections (see Figure 18 for location of profiles) showing the top and bottom of the Sand Unit (note that horizontal scale is in meters and vertical is in feet).

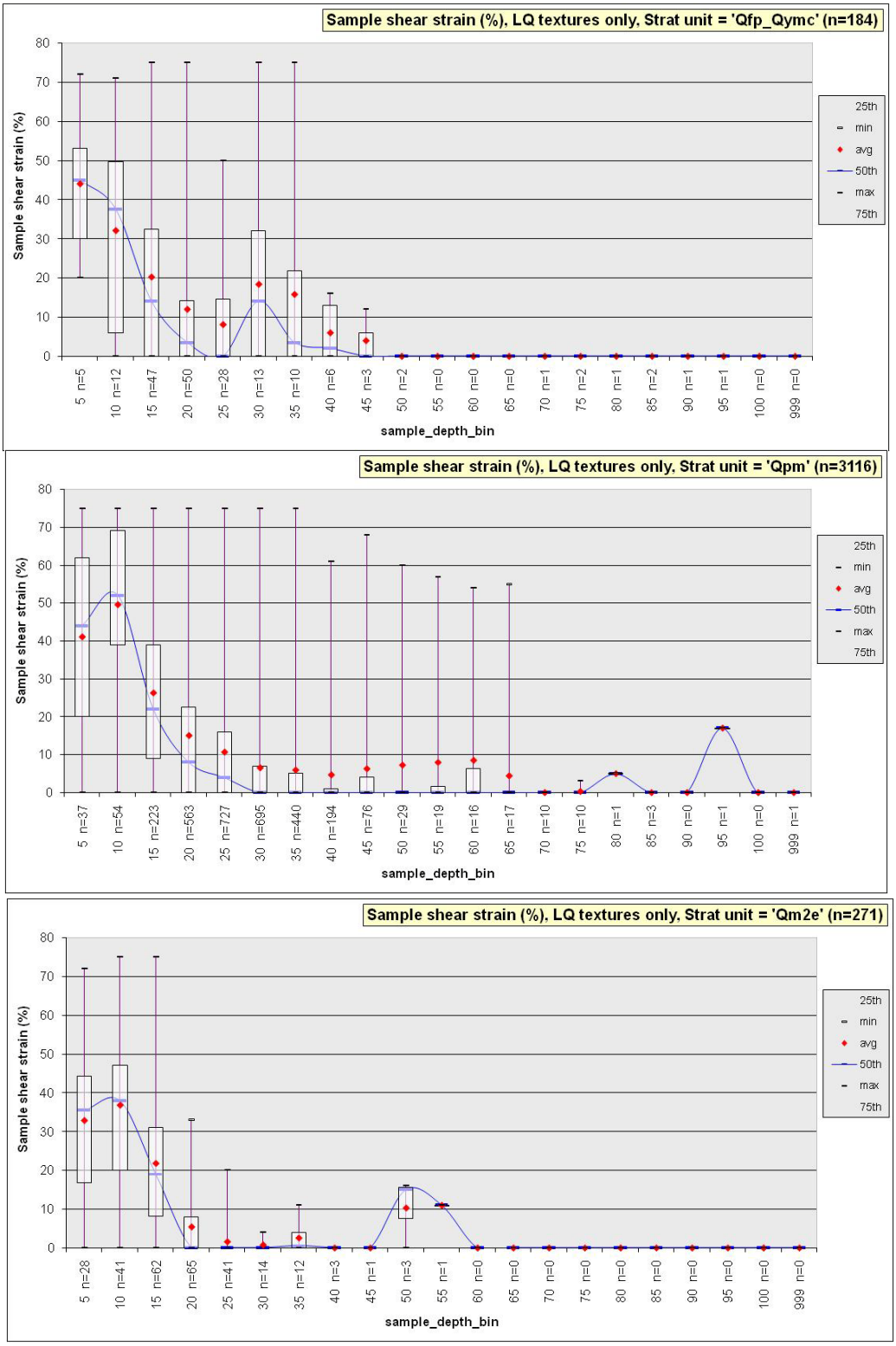

Figure 20. Box and whisker plots and shear strain vs. depth curves for each liquefaction-deformation susceptibility unit for an input shaking level of 0.2g. Boxes represent first and second quartiles, median is blue horizontal bar and mean the red dot in each box. Whiskers represent range of data values.

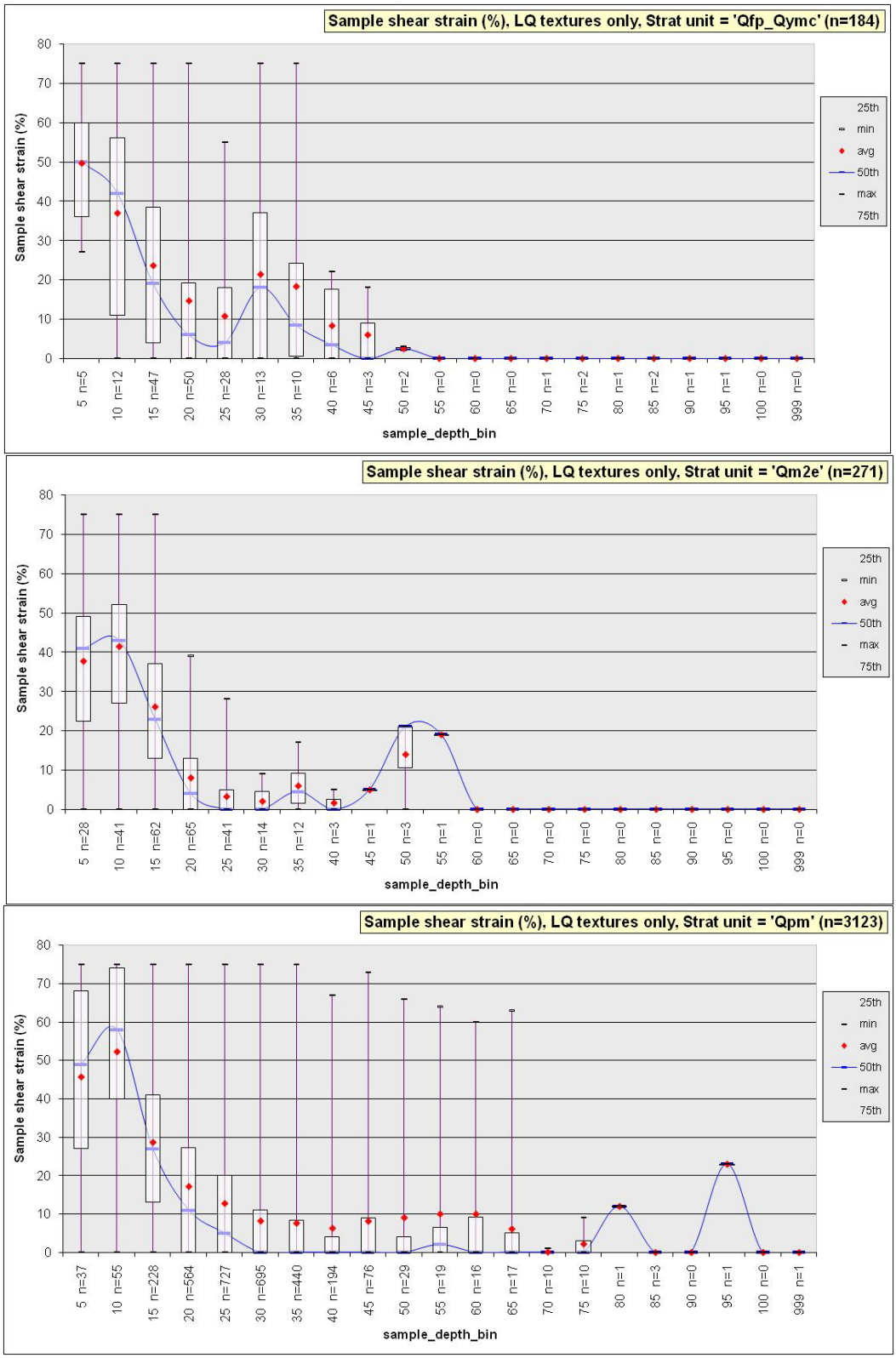

Figure 21. Box and whisker plots and shear strain vs. Depth curves for each liquefaction-deformation susceptibility unit for an input shaking level of 0.3g. Boxes represent first and second quartiles, median is blue horizontal bar and mean the red dot in each box. Whiskers represent range of data values.

Based on the significance results, the final sets of strain potential curves are hybrid: 1) consisting of the susceptibility-unit curves for the upper 30 feet, and 2) based on all of the SPT measurements (without grouping borehole data by susceptibility units) below 30 feet. The grouped differences are not significant below 30 feet, so we do not believe it is meaningful to use that portion of the curves that is based on too few measurements. Lumping all of the SPT measurements below this depth increases the sample dataset, and yields better estimates of the true population median and quartiles for strain.

Depth	Shear Strain @ 0.20g			Shear Strain @ 0.30g		
(ft)	H	p	Significant?	H	p	Significant?
0-5	1.843	0.398	N	1.930	0.381	N
5-10	7.092	0.029	Y	6.789	0.034	Y
10-15	6.497	0.039	Y	3.750	0.153	N
15-20	20.783	0.000	Y	13.028	0.001	Y
20-25	20.308	0.000	Y	12.753	0.002	Y
25-30	8.135	0.017	Y	7.476	0.024	Y
30-35	3.903	0.142	N	7.202	0.027	Y
35-40	2.691	0.260	N	0.933	0.627	N
40-45	0.406	0.816	N	0.865	0.649	N
45-50	2.427	0.297	N	1.856	0.395	N
50-55	16	0.165	N	16.000	0.235	N
55-60			NULL			NULL
60-65			NULL			NULL
65-70	5.5	1.000	N	5.000	0.763	N
70-75	9	0.655	N	7.000	0.396	N
75-80	0	0.317	N	0.000	0.317	N
80-85	4	1.000	N	4.000	1	N
85-90			NULL			NULL
90-95	0	0.317		0.000	0.317	N
95-100			NULL			NULL

Table 4. Kruskal-Wallis H-test for significant differences between liquefaction-deformation potential curves for three liquefaction-deformation susceptibility units (H – test value, p probability of random occurrence, critical H-value for df=2: 5.99, yellow indicates region of significant difference).

The final liquefaction-deformation potential functions are shown in Figures 22 and 23. These curves represent the hazard potential, and are used with grids of ground shaking, liquefaction – deformation susceptibility, top and bottom of liquefiable material grids to estimate displacement potential index. Grids of ground shaking and susceptibility were used to select the appropriate strain curve, which was then integrated over the top and bottom limits of the liquefiable unit at each grid location to estimate displacement index.

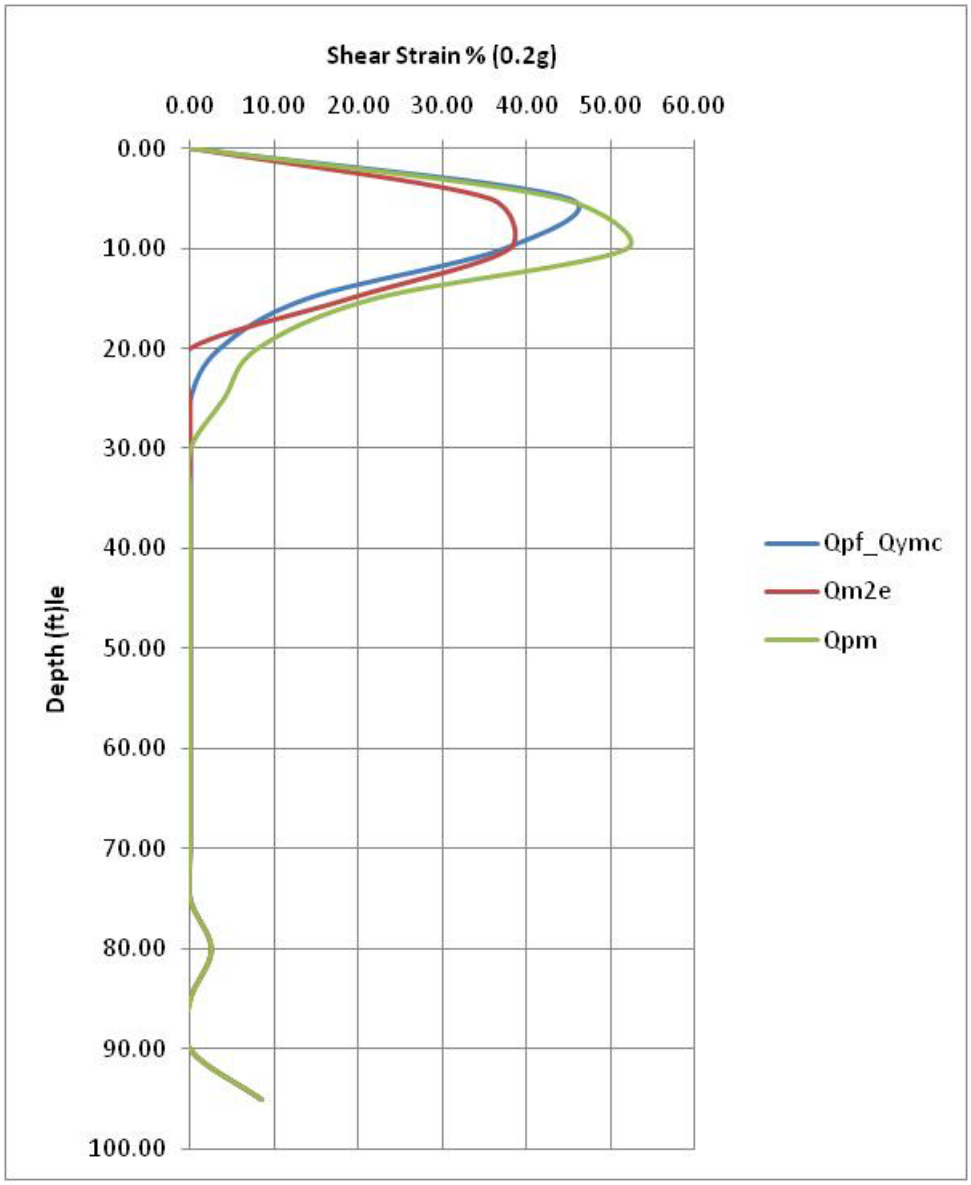

Figure 22. Shear-Strain vs. depth density curves for principal susceptibility units shaken at 0.2g duration-weighted peak horizontal ground acceleration. Selecting the appropriate curve and integrating over the depth to top and bottom of liquefiable layers provides an estimate of lateral displacement potential index at a given location. Similar curves were computed, and estimates made for volumetric-reconsolidation potential index.

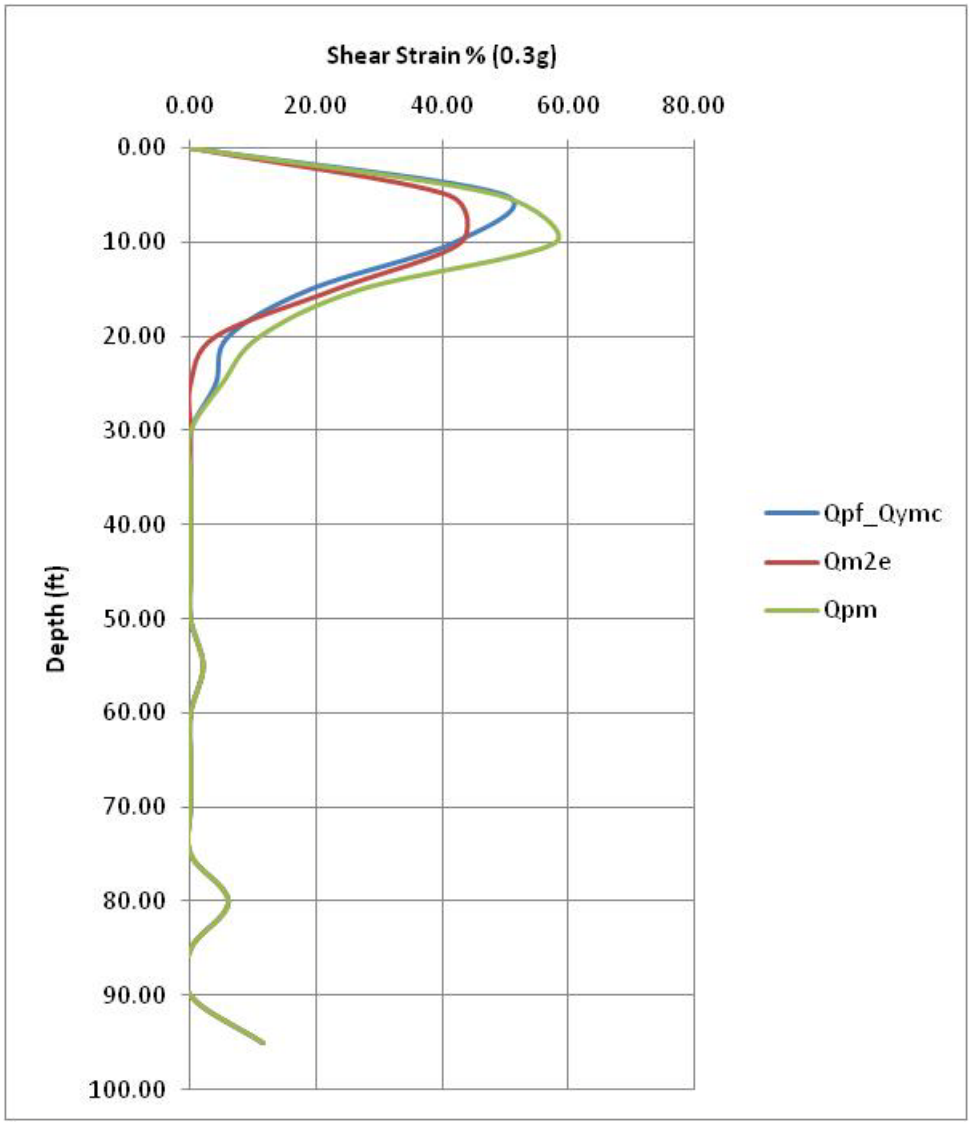

Figure 23. Shear-Strain vs. depth density curves for the principal liquefaction-deformation susceptibility units shaken at 0.3g duration-weighted peak horizontal ground acceleration. Selecting the appropriate curve and integrating over the depth to top and bottom of liquefiable layers provides an estimate of lateral displacement potential index at a given location. Similar curves were computed, and estimates made for lateral displacement potential index.

3.2.2 Liquefaction Deformation Hazard Maps

Using the liquefaction susceptibility and ground shaking maps, and the corresponding shear- and volumetric- reconsolidation-strain density curves, we have produced liquefaction hazard potential maps of the native geologic materials shown in Figures 24-27. Figures 24 and 26 show the continuous deformation-index fields while Figures 25 and 27 show deformation interval ranges and contours (isopleth). The overall pattern of hazard is similar for both deformation modes, which is to be expected since the hazard is driven by the thickness of

liquefiable sediment that is greatest near the center of the study area (see sand isopach map in Figure 18).

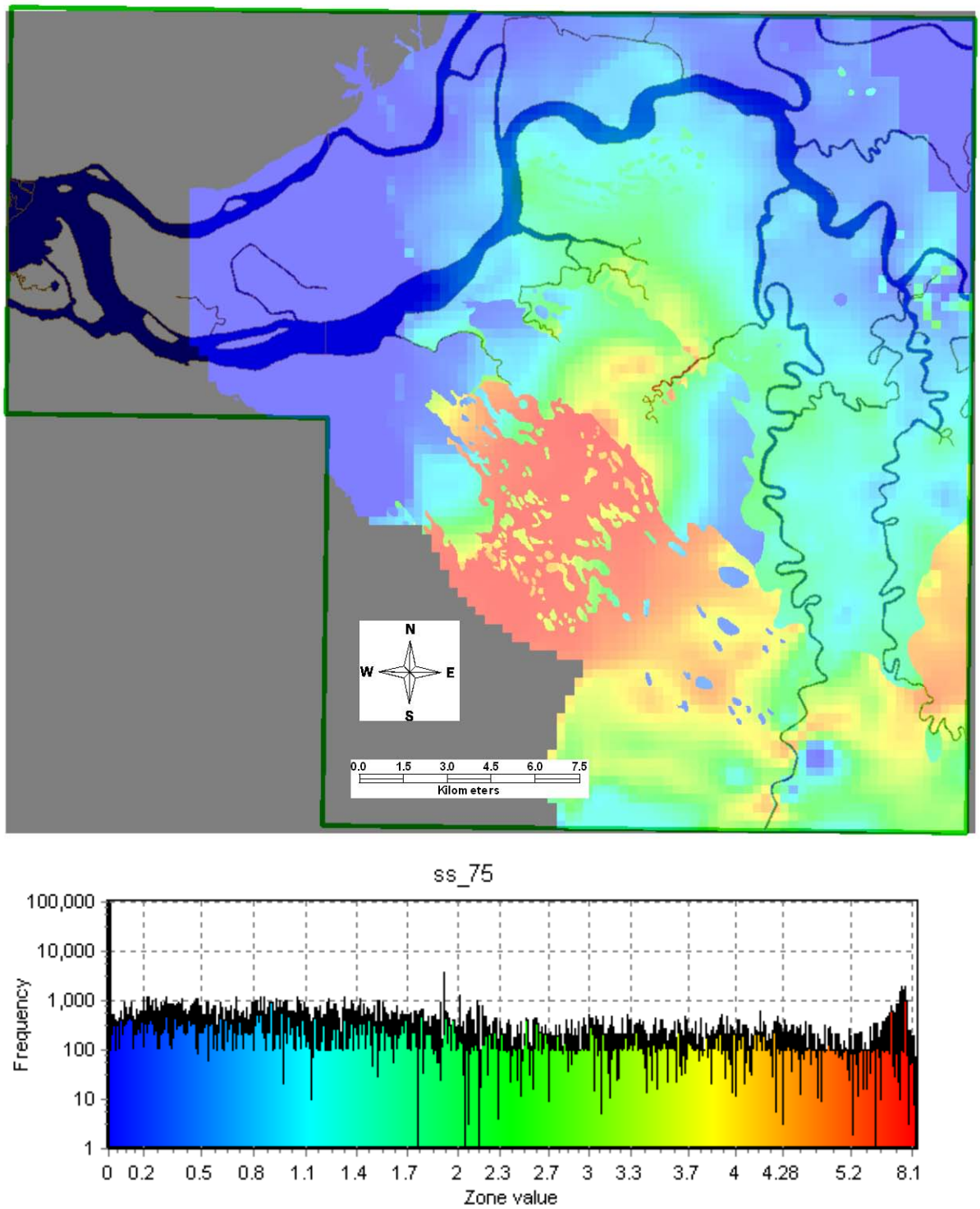

Figure 24. Lateral displacement potential index (3rd Quartile) over the study area. The legend is a frequency histogram as described in the caption for Figure 14 (zone value is displacement index in feet).

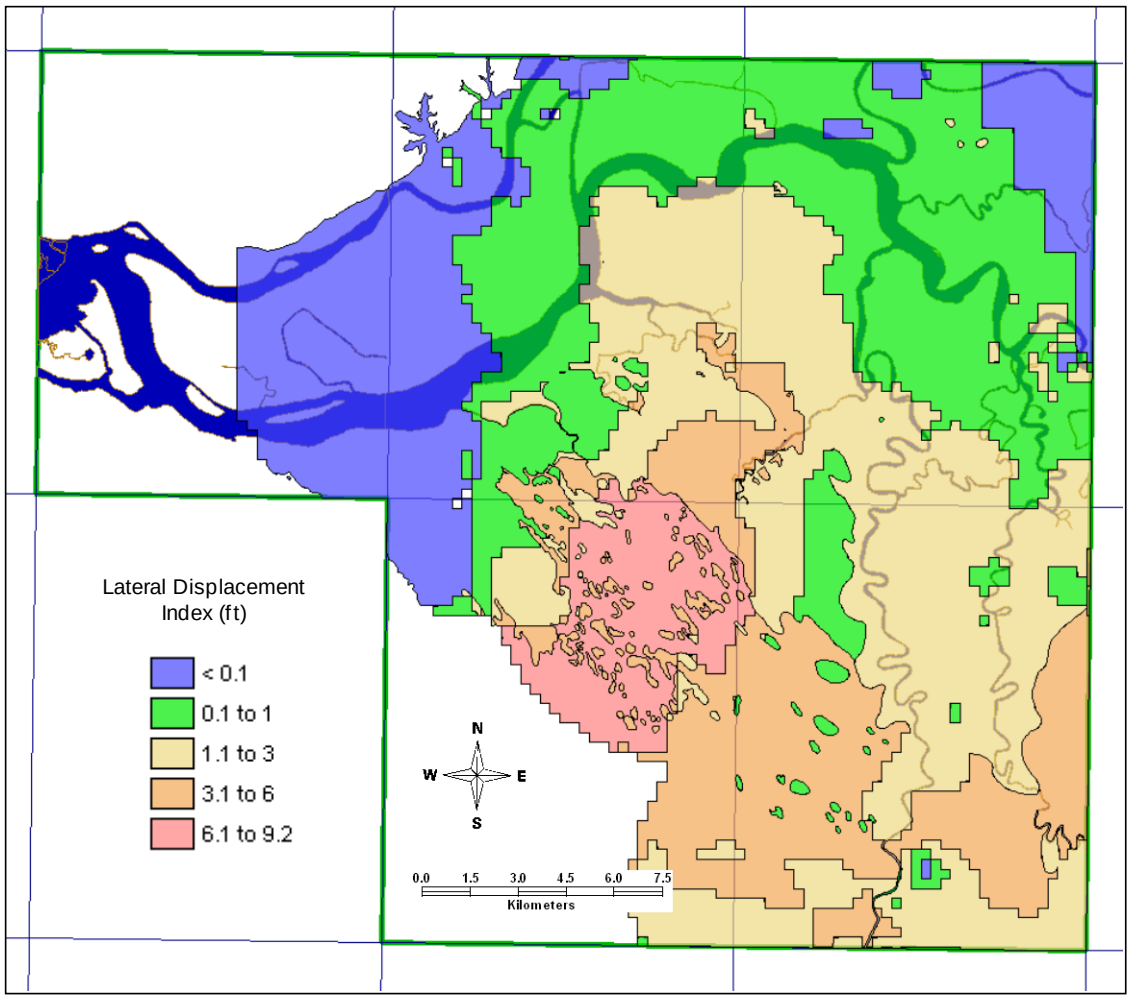

Figure 25. Liquefaction hazard map showing intervals of lateral displacement potential index in feet. Note that the first two intervals range to 1.0 foot (blue and green), while values greater than 1 are in intervals of 3 feet. The gridlines are boundaries of the 7.5' quadrangles identified in Figure 1 for reference.

It is important to note that the maps portray relative hazard in terms of a displacement index, not actual expected displacements, which would require consideration of static driving stresses (see discussion in Section 4.2).

Note that Figure 25 portrays lateral displacement potential index in intervals of 3 feet except for the first two intervals ranging to 1 foot. This is done because common slab foundations can be economically engineered to withstand minor displacements of a few inches, whereas larger displacements usually require more costly foundation designs or extensive site remediation. Also, note that the vertical deformation shown in Figures 26 and 27 does not represent total settlement, which must also include the component of vertical displacement that accompanies lateral movement of material caused by shear failure. That component was not estimated in this study. Instead, the map represents reconsolidation potential due to volumetric strain only. As is evident from both types of deformation shown in Figures 24 through 27, the overall areal pattern of hazard is very similar.

Another noteworthy feature of the hazard maps is that little or no deformation hazard is indicated north and northwest of the central study area, along the Sacramento River and San Joaquin River. This is because the sand deposits are much deeper, being overlain by up to more than 50 feet of non-liquefiable peat and organic mud (see Figure 17). Even though the unit weight of peat deposits is only about 65% of the unit weight of sands and silts, the thickness of overburden is sufficient to reduce the liquefaction susceptibility of underlying sands to zero or negligible levels (see Figures 20–23).

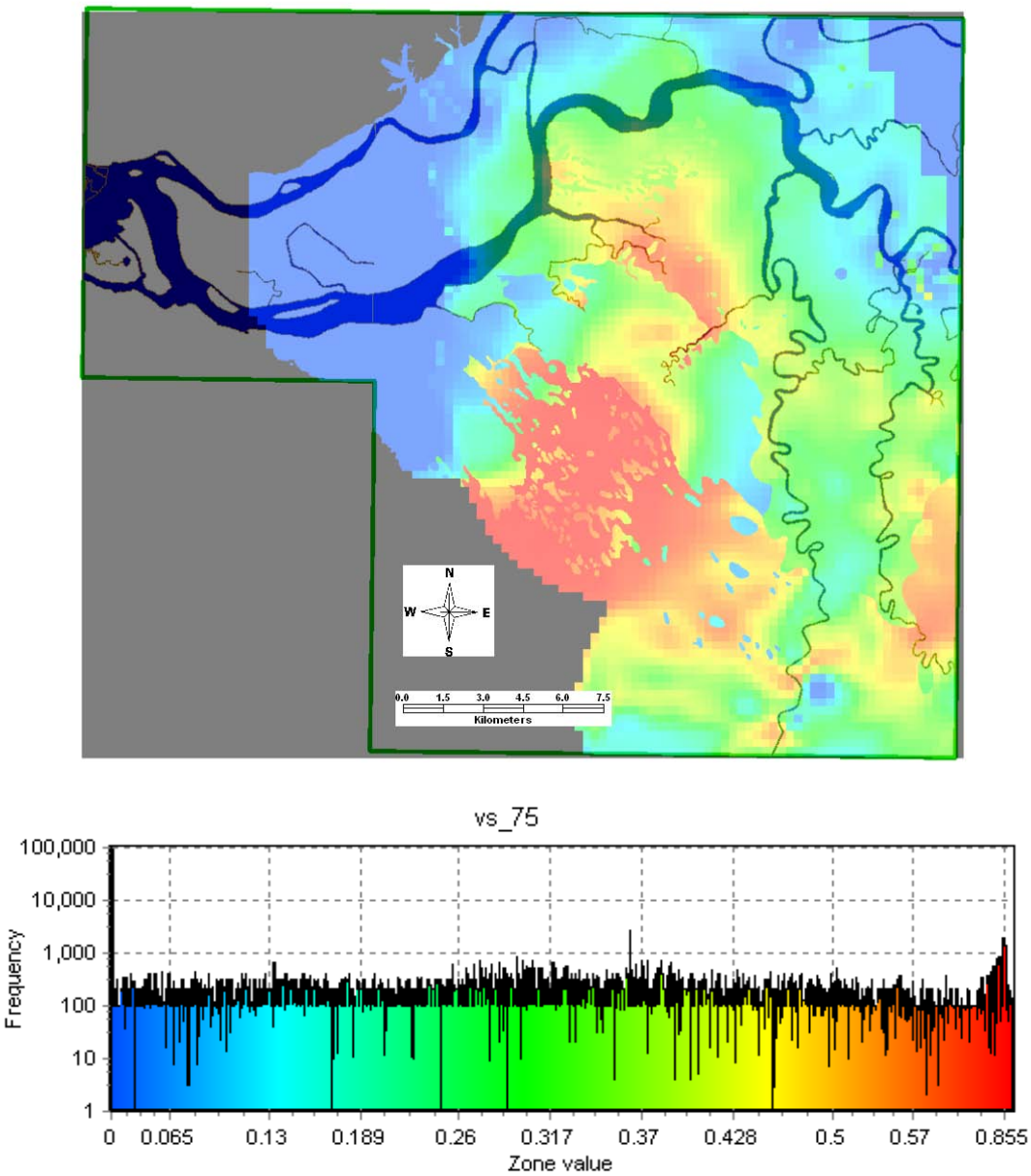

Figure 26. Volumetric Reconsolidation Index (3rd Quartile) over the study area. The legend is a frequency histogram as described in the caption for Figure 14 (zone value is volumetric reconsolidation index in feet).

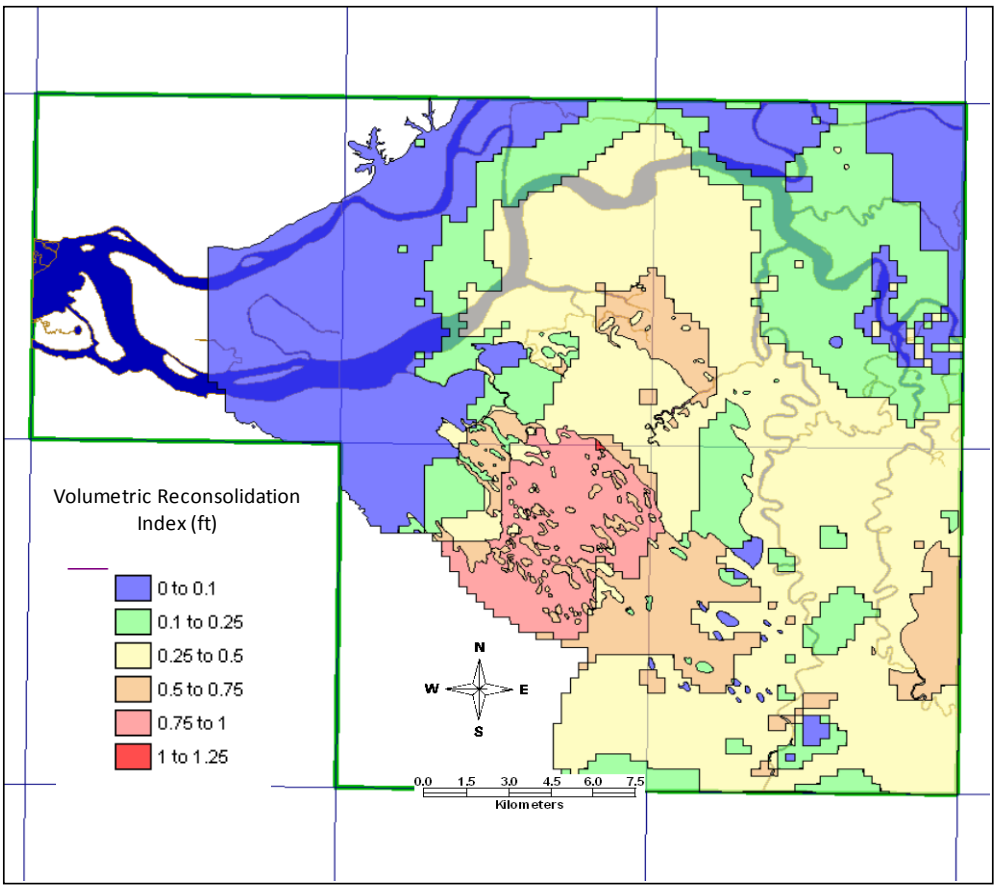

Figure 27. Liquefaction Hazard Map showing intervals of volumetric-reconsolidation index in feet. The gridlines are boundaries of the 7.5' quadrangles identified in Figure 1 for reference.

Also noteworthy are areas to the east portion of the study area, along the Old River and Middle River north-south tributaries of the San Joaquin River (Bouldin Island and Woodward Island quadrangles), where thickness of peat diminishes but the depth to top of liquefiable sands increases eastward. Deformation potential hazard is moderate along Old River and the southern extent of the Middle River, but is low along the northern extent of the Middle River; the latter because the strain potential diminishes at depths beyond 20 feet, which is where the sands lie in that part of the area (see profile B-B' Figures 18 and 19, and Figure 22).

1 Discussion

1.1 Significance of Results

Results of this project demonstrate a new approach to mapping liquefaction hazard based on potential for ground displacement when an abundance of geotechnical borings are available that are broadly distributed. The method relies on relationships that have been developed from empirical observation of lateral spreading for large strains, and from laboratory soil testing for small strains, between $N_{1,60,cs}$ and shear- and volumetric-reconsolidation strains. The

advantage of this method is that the hazard depicted reflects the potential for damaging ground movement rather than simply the triggering of liquefaction, without any indication of the severity of ground movement. Thus the range of hazard severity reflects the potential for structural/foundation damage, which makes the new method a better candidate to use as a policy instrument for land-use and construction decisions. The method is useful where liquefiable materials at depth have lateral continuity that permits interpolation of liquefaction-prone stratigraphy over the area of study.

Methods of borehole log correlation and subsurface stratigraphic mapping are well established having been developed over decades of hydrocarbon and mining exploration. The capability to accurately map thickness of sand- and silt-prone facies allows for a more accurate estimation (interpolation) of ground displacement and its uncertainty over the region if the distribution of *in situ* penetration testing of soils is dense enough to permit the spatial variation of earthquake-induced permanent strains to be reasonably characterized.

Compared to the method of analysis originally proposed for this study and described in the introduction, we believe that the new method is complimentary, and reduces overall uncertainty by reducing the epistemic component; incorporating more knowledge of the distribution of liquefaction-prone sediments into the analysis when possible. Although only a single subsurface liquefiable unit was ultimately used with the new methodology in this study, the procedure could, in principle, be applied to any number of discrete liquefiable layers in a stratigraphic model.

While the metric used in this study to portray liquefaction hazard is not a true estimate of expected deformation, the “strain indices” do reflect the variability of geotechnical soil properties relevant to the physics of earthquake-induced liquefaction. Consequently, the hazard maps do portray an improved estimate of hazard variability over the study area, which can allow one to focus on areas where the hazard is greatest and may need detailed site investigation for engineering projects. It is an improvement over previous mapping methods where the level of hazard detail is predominantly defined by stratigraphic unit formation boundaries.

4.2 Limitations

Caution should be exercised when interpreting the liquefaction hazard maps developed in this study for several reasons: 1) use of “strain potential indices” as a definition of hazard, and the inherent limitations it represents, 2) the variable quantity and quality of penetration data used in this analysis, 3) the adequacy of borehole sampling over the study area and its suitability for subsurface stratigraphic correlation and statistical analysis for characterizing the liquefaction behavior of sediments, and 4) the appropriateness of assumptions made and the methods employed.

The deformation parameters employed in this analysis are considered “indices” because they are based on algorithms developed from laboratory measurements of clean sands (for low strain) and back analysis of observations of large ground displacements (for high strain) caused by earthquakes around the world. They are reasonable relative first-order estimates of what are considered “limiting strains”, defined in the laboratory as maximum strains induced by 15 cycles of uniform cyclic loading without significant static driving stresses (Seed et al., 2003).

Conceptually, limiting strain has been described as the shear strain required for dilatent re-stiffening (Seed et al., 2003), which places an upper bound on how much displacement can occur before liquefaction shuts down and mass movement ceases. Thus, the index values represent rough upper bounds, which may or may not be reached since lateral displacement in the field depends on contributions from static driving stresses that vary over the study area depending on the geometry of the terrain and mode of failure for conditions of sloping ground or proximity to a free face. These factors were not evaluated in this study, so the resulting hazard indices may be a conservative representation of actual hazard. The DRMS evaluation of levee vulnerability does consider the native materials directly beneath the levees, and the presence of the channel free-face, so that component of Delta hazard is already available. Although the displacement algorithm of Faris (2006) does include slope gradient as a proxy for static driving stress, the Delta region is nearly flat, and the resolution of available topographic data over the region is insufficient to reliably estimate very gentle slopes. Thus, inclusion of that parameter is more suited for site-specific liquefaction hazard analysis.

It must be understood that the maps presented herein represent deformation hazard for earthquake-induced liquefaction only. Ground deformation during an earthquake may actually be greater than that identified, and may occur in areas not susceptible to liquefaction as a result of shear failure of the soft organic clays. Moreover, the maps do not show liquefaction-deformation potential of the levees as the objective of this project was to evaluate the native deposits only, which had not been evaluated and mapped regionally. The DRMS project focuses on an engineering evaluation of levee stability, including the underlying natural levee foundation material using more sophisticated analysis code for site-specific evaluation.

4.2.1 Data

The present study began with a database of previously interpreted soil stratigraphy from available boring logs acquired during decades of investigation by many different entities, using a variety of tools and methods. Considering sampling adequacy *horizontally* over the study area, the data are “clustered” along the levees and not well-distributed geographically (see Figure 5). This distribution is not favorable to areal interpolation, which lowers the reliability of interpreted structural elevations of subsurface lithologic horizons. Considering the adequacy of sampling *vertically*, Figure 28 shows the depth distribution of the boreholes, which indicates that the majority of borings are less than 50 feet total depth with the most common total depth in the 25 foot range. This puts constraints on the reliability of the statistical estimates of strain as a function of depth for different sedimentary units, particularly for depths beyond 30 feet (see Figures 20 and 21).

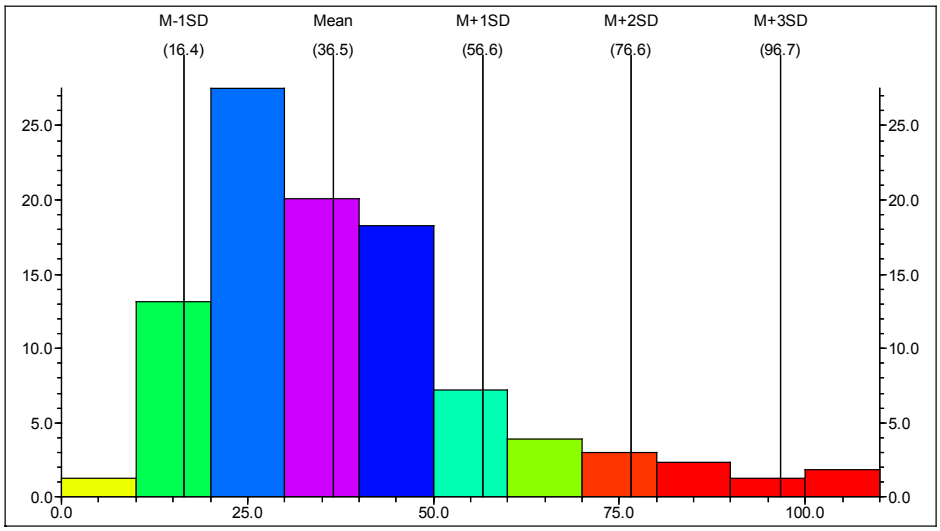

Figure 28. Histogram of borehole total depth for borings used in this study showing boring count on the vertical axis (percent left side, number right side) and the depth range in feet on the lower horizontal axis. Upper horizontal axis shows the mean and standard deviations.

The majority of penetration tests were made using a non-standard sampling tool (1 inch diameter), and not necessarily conducted according to tests for liquefaction analysis (ASTM D 6066). We applied corrections for all non-standard tools (Burmister, 1962), but the additional error in this approach is unknown. Total uncertainty (coefficient of variation) in true SPT measurements has been cited in the range of 15-45% (Kulhawy, 2004).

Original lithology calls were not used, but instead we used interpreted simplifications from the DRMS analysis. Because these simplifications were a result of a previous liquefaction analysis in the DRMS study, we believe they likely represent a reasonable classification of liquefiable and non-liquefiable materials in the borings.

Ground motion data used in this project were acquired on a 1 kilometer grid using the 10% in 50 years 2002 joint USGS/CGS PSHA model corrected for alluvial site conditions. We chose these parameters to be consistent with that level used in conventional building construction and currently used for delineation of official seismic hazard zones according to California law. Aleatory uncertainty in the estimates of PGA is integrated as part of the probabilistic results from a PSHA model. A new ground shaking hazard model has been released that incorporates the NGA attenuation relations, which may change the results of this project (Petersen et al., 2008). The appropriateness of the new model is currently under evaluation for replacement in the procedures for mandated hazard zoning.

4.2.2 Method

In addition to the uncertainties in the data, there are uncertainties in the methods used to analyze liquefaction triggering, in estimating strain, in mapping the areal distribution and thickness of subsurface liquefiable deposits, and in reclassifying the mapped surface geology

and assigning a strain response function to the new “liquefaction-deformation susceptibility units.” Regarding triggering analysis, nearly all of the boring logs were taken in boreholes on levees, and were modified in order to be used to evaluate the liquefaction susceptibility of the adjacent native materials that extend beneath the levees. To do this, we first corrected the field measurements to “standard conditions” using the method of Youd and others, (2001), but when estimating liquefaction potential given the earthquake loading conditions, we effectively removed the levee material (overburden stress) and adjusted soil unit depth accordingly as if the boring locations were on level, native ground as described previously. We also assumed 100% saturation since depth to ground water in the Delta region is at the surface or within a few feet. So, in addition to all of the limitations and uncertainties of the “simplified method” of liquefaction triggering potential, the adjustment of borehole data contributes more uncertainty into the deformation estimation process. We do not know what additional uncertainty is added, but the adjustment procedure was applied uniformly to all levee borings. Thus, there may be a resulting bias in these results relative to results from borings acquired off levees, on level ground.

We used the relationships between shear- and volumetric reconsolidation strain verses cyclic stress ratio and fines corrected penetration resistance of Wu (2002) as modified by Faris (2004) for calculating strain. Neither relation provides uncertainty bounds on the strain curves, precluding the possibility of propagating uncertainties through the strain estimation process and the potential for a fully probabilistic analysis. Regardless, such an analysis would only be meaningful if the hazard were characterized by estimates of actual expected displacements instead of an index of deformation. We believe the hazard values presented do represent relative severity of potential deformation from liquefaction.

The methodology developed in this study also strongly depends on the extent to which the subsurface stratigraphy can be correlated over an area. Only two working units, the peat-soft organics and middle sand working units were traceable over a large portion of the study area. Interbedded sand facies and non-liquefiable sediments occur intermittently throughout the area above the peat and below the working interval we call middle sand. The upper sand facies were too discontinuous to define spatially given the borehole distribution, and were not included in the hazard analysis. This means that locally, at large scale, highly liquefiable materials could lie near the ground surface at a particular site where our maps indicate a low hazard. Conversely, thickness estimates of liquefiable units are biased high, because they contain interbedded and discontinuous non-liquefiable sediments of minor thickness. Engineering behavior of these sediments was ignored and their presence was included in thickness estimates as sand. To obtain a total thickness of potentially liquefiable material we simply combined the middle sand working unit thickness with an isopach of the lower sand unit to yield a single sand unit having a revised lower base over which to integrate the strain functions for estimating displacements. Thus the conservatism in thickness estimates adds additional conservatism in the resulting hazard estimates.

Finally, due to the limited scope of this project we did not explore sensitivity of the surfaces interpolated from the borehole stratigraphic analysis to the various analytical interpolation

techniques. We employed the inverse distance weighting algorithm; however, other methods such as kriging may be more accurate given the clustered nature of the borehole data.

4.3 Recommendations for Further Work

Although the primary goal of this project was to further develop and test a new methodology of mapping liquefaction hazard, some of the limitations described above can be reduced or eliminated by further work, which could improve the reliability of the liquefaction hazard map resulting from this study. Suggestions for further work are listed as follows:

1. The reliability of the results in this study is strongly dependent on the validity the method used to correct levee boring logs to represent the adjacent natural material. One way to evaluate how well the method works is to select a subset of the modified borehole results that have nearby off-levee boreholes and compare them with the actual unaltered borings. This would provide a rough check on the validity of the “modified” borings.
2. The methodology should be enhanced to carry all uncertainties through a full probabilistic analysis. This would require uncertainty estimates on the relationships used to estimate shear- and volumetric- reconsolidation strains, a probabilistic liquefaction triggering analysis, including a probabilistic combination of multiple potentially liquefiable layers in a borehole.
3. To provide some idea of uncertainty in the present study results, liquefaction hazard maps can be prepared based on the first and third quartile strain relationships shown in Figures 18 and 19. Although not representative of total uncertainty, this would demonstrate the component of spatial uncertainty of hazard introduced by the statistical averaging of borehole strain estimates based on the reclassification and grouping of borehole data by surface geology.
4. To produce a liquefaction hazard map for practical use in the Delta, the ground shaking input should consider the risk level appropriate for the intended decision making…conversion of land use to housing, potential impact to infrastructure (lifelines, etc.). The NGA study attenuation models have now been incorporated into the NEHRP shaking hazard model, and could possibly be used to improve the hazard estimates of this study.

There still remains the problem of inadequate spatial sampling of soils (density, depth, and areal coverage) that, when corrected, can improve capture of scattered isolated pockets of liquefiable near-surface sediment capable of causing damaging ground deformation. Future construction on Delta land should be preceded by additional borehole sampling for parcels under development or at lifeline construction sites to identify such local site-specific hazard. Additionally, such investigations for overall ground deformation hazard should include assessing potential for soft-clay failure.

5 References

Atwater, B.F. (1982). “Geologic Maps of the Sacramento-San Joaquin Delta, California,” USGS MAP MF-1401, scale 1:2,400.

Burmister, D.M. (1962). “Physical, Stress-Strain, and Strength Responses of Granular Soils,” ASTM Spec. Tech. Pub. No. 322: 67-97.

CALFED Bay-Delta Program (2000). “Seismic Vulnerability of the Sacramento-San Joaquin Delta Levees: Levees and Channels Technical Team/Seismic Vulnerability Sub-Team”, 59p.

Cetin, K.O., Seed, R.B., Der Kiureghian, A., Tokimatsu, K., Harder, L.F., Kayen, R.E., and Moss, R.E.S. (2004). “Standard Penetration Test-based probabilistic and deterministic assessment of seismic soil liquefaction potential.” Journal of the Geotechnical and Geoenvironmental Engineering, 130(12):1314–1340.

Faris, A. (2004). “Probabilistic Models for Engineering Assessment of Liquefaction-Induced Lateral Spreading Displacements,” PhD. Thesis, University of California, Berkeley, California,184 p.

Faris, A.T., Seed, R. B., Kayen, R.E., and Wu, J. (2006). “A Semi-Empirical Model for the Estimation of Maximum Horizontal Displacement Due to Liquefaction-Induced Lateral Spreading,” Proceedings 8th U.S. Conference on Earthquake Engineering, April 18-22, 2006, San Francisco, California, Paper No. 1323, 10 p.

Hitchcock, C.S., Helley, E.J., and Givler, R.W. (2005). Geomorphic and Geologic Mapping for Restoration Planning Sacramento-San Joaquin Delta Region: William Lettis & Associates, Walnut Creek CA, 32 p (includes DVD Digital Data).

Holzer, T.L., Bennett, M.J., Noce, T.E., Padovani, A.C., and Tinsley, J.C., III (2006). “Liquefaction hazard mapping with LPI in the greater Oakland, California, area.” Earthquake Spectra, 22(3): 693-708.

Ishihara, K. and Yoshimine, M. (1992). “Evaluation of Settlements in Sand Deposits Following Liquefaction During Earthquakes,” Soils and Foundations, V. 32, No.1: 173-188.

Knudsen, K.L., Rosinski, A., and Seed, R.B. (2004a). "Production of Regional Liquefaction-Induced Deformation Maps." Proceedings, 11th International Conference on Soil Dynamics and Earthquake Engineering and the 3rd International Conference on Earthquake Geotechnical Engineering (a jointly convened conference pairing), University of California at Berkeley, January 2004.

Knudsen, K.L., Rosinski, A., Wiegers, M.O., Real, C.R., Wu, J., and Seed, R.B (2004b). “Investigation of Methods to Produce Regional Maps of Liquefaction-Induced Deformation.” Pacific Earthquake Engineering Research Center, Final Report 3G01-FR[1]: 61 p.

Kulhawy, F.H. (2004). “Estimation of Soil Properties for Foundation Design,” in, Short Course Lecture Notes, ASCE Geo-Institute Conference, Los Angeles, CA July 27, 2004.

Real, C.R., Knudsen, K.L., and Woods, M.O. (2008). “A Deformation-Based Approach for Mapping Earthquake-Induced Liquefaction Hazard.” ASCE Geotechnical Special Publication No. 181: 10 p.

Real, C.R. (2002). “California’s Seismic Hazards Mapping Act: Geoscience and Public Policy.” in, Bobrowsky, P.T., ed., Geoenvironmental Mapping: Methods Theory and Practice, A.A. Balkema, Exton, PA: 93-120.

Real, C.R., Petersen, M.D., McCrink, T.P. and Cramer, C.H. (2000). “Seismic Hazard Deaggregation in zoning earthquake-induced ground failures in southern California,” Proceedings of the Sixth International Conference on Seismic Zonation, November 12-15, Palm Springs, California, (CD-ROM), EERI, Oakland, CA.

Rosinski, A., Knudsen, K.L., Wu, J., Seed, R.B., and Real, C.R. (2004). “Development of Regional Liquefaction-Induced Deformation Hazard Maps.” in, Yegian, M.K. and Kavazanjian, E., eds., Geotechnical Engineering for Transportation Projects, ASCE Geotechnical Special Publication No. 126: 797-806.

Seed, R.B., Cetin, K.O, Moss, R.E.S., Kammerer, A.M., Wu, J., Pestana, J.M., Riemer, M.F., Sancio, R.B., Bray, J.D., Kayen, R.E., and Faris, A. (2003). “Recent Advances in Soil Liquefaction Engineering: A Unified and Consistent Framework,” 26th annual ASCE Los Angeles Geotechnical Spring Seminar Keynote Presentation, H.M.S. Queen Mary, Long Beach California, April 30, 2003, 71 p.

Shamoto, T., Shang, J.M., and Tokimatsu, K. (1998). “Methods for evaluating residual post-liquefaction ground settlement and horizontal displacement,” Soils and Foundations, Special Issue, 69-83.

Shlemon, R.J. (1971). “The Quaternary Deltaic and Channel System in the Central Great Valley, California: Annals of the Association of American Geographers,” v.61, No.3: 427-441.

Storey, J.A., Wessels, V.E., and Wolfe, J.A. (1966). “Radiocarbon Dating of Recent Sediments in San Francisco Bay,” California Division of Mines and Geology, Mineral Information Service, V.19, No.3: 47-50.

Tokimatsu, K. and Seed, H.B. (1987). “Evaluation of Settlements in Sands due to Earthquake Shaking,” Journal of Geotechnical Engineering, V. 113, No. 8, p 861-878.

URS Corp (2008). “Technical Memorandum: Delta Risk Management Strategy (DRMS) Phase 1, Levee Vulnerability Technical Memorandum – Final,” 103p.

Witter, R.C., Knudsen, K.L, Sowers, J.M., Wentworth, C.M., Koehler, R.D., Randolph, C.E., Brooks, S.K., and Gans, K.D. (2006). “Maps of Quaternary deposits and liquefaction susceptibility in the central San Francisco Bay region, California.” U.S. Geological Survey Open-File Report 2006-1037.

Wu, J. (2002). Liquefaction Triggering and Post Liquefaction Deformations of Monterey 0/30 Sand Under Uni-Directional Cyclic Simple Shear Loading. PhD. Thesis, University of California, Berkeley, CA.

Youd, T.L. and Perkins (1978). “Mapping of Liquefaction Induced Ground Failure Potential.” Journal of Geotechnical Engineering Division, ASCE, 104(4): 433-446.

6 Plates

6.1 Paleo-land surface on the base of the peat-soft organics

6.2 Large-scale geologic map of paleo-land surface

7 Acknowledgments

Terilee McGuire and Marvin Woods of the California Geological survey assisted in development of the project database. Marvin Woods and Robert Moskovitz (CGS) helped develop the analysis tools, performed the necessary code development, and helped perform analysis of the boring log data. Susan Olig (URS) performed much of the interpretation of subsurface data for development of the pale0-land surface maps; Douglas Wright (URS) provided GIS support in this endeavor. The URS DRMS team kindly provided and explained the boring log information used in this study. We thank Christopher Hitchcock of William Lettis & Associates for providing digital map data from their 2005 CALFED study of the Delta.